

Abstract

Contents

1	Introduction	1
2	Theoretical background	5
2.1	Continuum electro-elasticity	5
2.2	Entropy-driven electro-elasticity of an isotropic polymer network	8
2.3	Phenomenological approach to electro-elasticity	12
3	Electro-elasticity of solutions and anisotropic networks of polymer molecules	14
3.1	First law of thermodynamics	14
3.2	One-dimensional systems of charges, dipoles, and molecular chains in an electric field	14
3.2.1	A single electric charge	15
3.2.2	Dipoles	16
3.2.3	Polymer molecule (chain)	18
3.3	Polymer molecules (chains) in electric field	22
3.3.1	Distribution of monomer orientation	23
3.4	An anisotropic network of polymer molecules	23
3.4.1	Deriving the properties of the polymer	28
4	Application to electrostatically biased network	31
4.1	Chain distribution	31
4.2	Monomer orientation	34
4.3	The free state	35
4.4	Material properties	37
4.5	The coupled response	38
5	Experimental work	40
5.1	Influence of uniaxial and biaxial stretching	40
5.2	Influence of electric field	42
5.2.1	Experimental setup	42
5.2.2	Results and discussion	44
6	Conclusions	45
	References	48
A	The first law of thermodynamics in terms of electric enthalpy	49

B Chain stress and deriving the chain end-to-end vector from the deformation gradient	52
C The initial guess for τ	53

List of Figures

1	A schematic description of the coordinate system $\{\hat{\mathbf{E}}, \hat{\mathbf{Y}}, \hat{\mathbf{Z}}\}$ and the applied spherical coordinates.	8
2	Schematic description of an arbitrary one dimensional system subjected to electromechanical excitation at its boundary.	14
3	Schematic description of a single charge subjected to an electric field. . . .	15
4	Schematic description of a single dipole consisting of two charges, Q^+ and Q^- , connected by a stiff rod in an electric field.	16
5	Schematic description of a dipole in an electric field.	17
6	The entropy of a polymer chain with uniaxial dipoles as a function of the normalized radius as $0 \leq \frac{r}{nl} \leq 1$ and $l = 100 \mu\text{m}$. The red continuous curve with circular markers corresponds to $n = 50$ and the brown curve with squares to $n = 100$. The dashed columns corresponds to the normalized radii in accordance with the results in section 3.2.3, $\frac{r}{nl} = \sqrt{\frac{2}{3}} \frac{1}{\sqrt{n}}$, and the dot-dashed columns to the results from random walk statistics, $\frac{r}{nl} = \frac{1}{\sqrt{n}}$. . .	32
7	The natural logarithm for the maximum number of configurations as a function of the electric field magnitude for chains with uniaxial dipoles at different inclinations. The blue curve with circular markers corresponds to $\Theta = \frac{\pi}{1000}$, the red curve with squares to $\Theta = \frac{\pi}{4}$ and the yellow curve with diamonds to $\Theta = \frac{\pi}{2}$	33
8	The most probable end-to-end length as a function of the electric field magnitude for chains with uniaxial dipoles at different inclinations. The blue curve with circular markers corresponds to $\Theta = \frac{\pi}{1000}$, the red curve with squares to $\Theta = \frac{\pi}{4}$ and the yellow curve with diamonds to $\Theta = \frac{\pi}{2}$	33
9	The size of the Lagrange multiplier τ , associated with the most probable radius as a function of the electric field magnitude for chains with uniaxial dipoles at different inclinations. The blue curve with circular markers corresponds to $\Theta = \frac{\pi}{1000}$, the red curve with squares to $\Theta = \frac{\pi}{4}$ and the yellow curve with diamonds to $\Theta = \frac{\pi}{2}$	33
10	The monomer distribution for a polymer chain of uniaxial dipoles. The magnitude of the electric field during the polymerization process is $E = 150 \frac{\text{MV}}{\text{m}}$. (a) Corresponds to the chain with the inclination $\Theta = \frac{\pi}{1000}$ and end-to-end length $r = 0.89 \sqrt{n} l$. (b) Corresponds to $\Theta = \frac{\pi}{4}$ and $r = 0.91 \sqrt{n} l$. (c) Corresponds to $\Theta = \frac{\pi}{2}$ and $r = 0.93 \sqrt{n} l$	34
11	The amorphous monomer distribution of a uniaxial dipole as $E = 150 \frac{\text{MV}}{\text{m}}$. According to the numerical analysis as $\tau = 0$ and identical to the results of the analytical analysis that was presented by ?.	35

12	The number of chains along each inclination as a function of the inclination relative to the direction of the electric field, $N(\Theta, \Phi = 0)$. The blue curve with circular markers corresponds to the isotropic polymer and the yellow curve with squares corresponds to the biased polymer.	35
13	The fractions of chains along each inclination as a function of the inclination to the direction of the electric field, $\nu(\Theta)$. The blue curve with circular markers corresponds to the isotropic polymer and the yellow curve with squares corresponds to the biased polymer.	36
14	$\sigma_{\text{Diff}} = \sigma_{\text{EE}} - \sigma_{\text{YY}}$ as a function of λ_0 after the removal of the electric field with the magnitude of $E = 150 \frac{\text{MV}}{\text{m}}$	37
15	The deviatoric mechanical stress as a function of the deformation ratio, λ . Dashed curves corresponds to the isotropic polymer, continuous curves to the biased polymer and the dot-dashed curves to a polymer described by the IED model. The blue curves corresponds to the normal stress in the direction of the electric field, $\sigma_{\text{EE}}^{\text{m}}$, and the red curves to the transverse stress, $\sigma_{\text{YY}}^{\text{m}} = \sigma_{\text{ZZ}}^{\text{m}}$	37
16	The susceptibilities of the polymers as a function of the electric field. The black dashed curve corresponds to the isotropic polymer, the black continuous curve to the biased polymer and the black dot-dashed line to a polymer described by the IED model. (the dashed and the continuous curves overlap).	38
17	The deformation in the direction of the electric field, λ , as a function of the magnitude of the electric field. The black dashed curve corresponds to the isotropic polymer, the black continuous curve to the biased polymer and the black dot-dashed curves to a polymer described by the IED model.	38
18	(a) The self constructed stretching device. (b) The C-clamp used as a parallel plate capacitor.	40
19	The relative permittivity measurements as functions of the percentage of surface area expansion. The dashed and dotted curves correspond to the analytical results [?], as n are estimated from the stretch at failure (n_f) and from fitting the analytical equations to the experimental results (n_e), respectively. (a) PDMS under uniaxial stretch. (b) VHB under uniaxial stretch. (c) VHB under biaxial stretch.	41
20	A schematic description of the experimental system.	42
21	The parts of the plate capacitore.	43
22	The permittivity measurements a functions of the electric field on the sample. The Blue dots corresponds to a relaxed sample and the red circles corresponds to the area pre-stretch of $A = 225\%$. (a) PDMS, (b) VHB.	44

List of Tables

- | | | |
|---|---|----|
| 1 | The number of monomers in a single chain for the case presented in Fig. 19. | 42 |
|---|---|----|

1 Introduction

(Note: Strong points for EAP use)

Dielectric elastomers (DEs) are polymers that are nonconductive but polarize and deform under electrostatic excitation. These lightweight and flexible polymers are readily available and may potentially be used as actuators in a wide variety of applications such as artificial muscles, energy-harvesting devices, micropumps, and soft robotics [?].

(Note: The microstructure and macrostructure of the EAP (polymer networks from chains and chains from monomers -> a polymer strip sandwiched between two electrodes))

At the microscopic level, DEs have a hierarchical structure of polymer-chain networks. A polymer chain is a long string of repeating dipolar monomers. At the macroscopic level, the essential part of a DE-based device is a thin, soft DE membrane sandwiched between two flexible electrodes. Upon applying an electric potential across the electrodes, the monomers react to the electric excitations while the DE membrane becomes thinner as a result of the attraction between the two oppositely charged electrodes. Simultaneously, the membrane area expands due to the Poisson effect. This process converts electrical energy into mechanical energy. The attractive features of dielectric elastomers include large strain, fast response, silent operation, low cost, and high efficiency [?].

(Note: The ratio between elastic moduli and dielectric moduli and its importance)

The electromechanical coupling in DEs is characterized by a quadratic dependence of the force between the electrodes on the applied electric potential [?]. In turn, the deformation depends on the force via the elastic moduli. Thus, the coupling depends on the ratio between the dielectric and elastic moduli. Flexible polymers typically have low dielectric moduli, whereas polymers with high dielectric moduli are generally stiff. Given that this ratio is relatively small, large electric potentials are needed to obtain non-negligible actuation.

(Note: electric breakdown and other failure mechanisms)

The requirement for high electric potential implies that the feasibility of these materials is limited by their dielectric strength, which is the electric potential beyond which electric current flows through the dielectric material [?]. Exceeding this electric potential results in what is known as electric breakdown or dielectric breakdown, in some cases transforming the insulator into an electric conductor. In general, dielectric breakdown may be a singular, cyclic, or continuous event [?]. Accurately predicting the occurrence of dielectric breakdown and its timing and position is not yet possible, essentially because it does not depend on a single cause but is a statistical product of several factors. The most notable factors are local defects such as voids or inclusions that locally decrease the DE thickness, increasing the local electric field and/or mechanical stresses [?]. In practice, the dielectric strength is measured experimentally [??] for a membrane with a

given thickness and with the requisite testing equipment [?]. ?? examined the failure mechanisms and the performance boundaries of DEs and showed that the performance of highly viscoelastic polymer membranes as DEs is governed by four key mechanisms: dielectric breakdown, current leakage, pull-in failure, and viscoelasticity.

(Note: The ratio between elastic moduli and dielectric moduli - low but can be improved)

One possible way to overcome dielectric breakdown is by reducing the electric potential currently required for non-negligible actuation, which can be done by improving the DE polarizability. Several previous works suggest that the low ratio of dielectric modulus to elastic modulus may be improved, which would enhance the electromechanical response. A common approach to improving this ratio involves inserting additional materials into the elastomer, which can result in a homogeneous or composite elastomer. One aspect of this approach involves embedding components with a higher dielectric constant (i.e., that can be classified as insulating or conducting) into a soft polymer [???]. ? presented such a method to enhance the electromechanical response of silicone elastomer networks by grafting molecules with high permanent dipoles to the crosslinking molecules. Through adjusting the crosslinking density, their method also provides direct control of the mechanical properties of the elastomer. Another aspect of the approach involves improving the actuation in DEs by appropriately adjusting their microstructure as periodic laminates [?????].

(Note: improving the response without changing the ratio between elastic moduli and dielectric moduli)

In contrast with the approach of improving the ratio of dielectric modulus to elastic modulus, several works, which mainly target soft robotics, have chosen to improve the responsiveness of DEs by adjusting the macroscopic structure of the actuators [????]. Recent works such as ? and ? have discussed soft electrohydraulic transducers, which are called “Peano-HASEL actuators” (hydraulically amplified self-healing electrostatic actuators). Such actuators combine the advantages of both fluidic actuators and electrostatic actuators and are comprised of pouches made of flexible dielectric polymer films, filled with a liquid dielectric and covered with compliant electrodes. Upon applying a voltage across the electrodes, they “zip” together because of the Maxwell stress, which displaces the liquid inside the pouch and thereby contracts the actuator [?].

(Note: Previous investigations of the polymer properties:)

(Note: Mechanical response)

The desire to adjust the DE ratio of dielectric modulus to elastic modulus motivates a multiscale inquiry of the mechanical, dielectric, and coupled properties of these materials. The response of polymers to purely mechanical loading across all scales has been extensively investigated. For example, ? investigated in detailed the macroscopic behavior of soft materials undergoing large deformations . ? used statistical mechanics to make a

pioneering analysis at the microscopic level, which resulted in a Langevin-based constitutive relation. This work led to a variety of multiscale models, such as the three-chain model [?] and the eight-chain model [?]. A similar analysis of mechanical systems was also presented by ?, ?, and ? for polymer networks with rubberlike elasticity. ? review the development of statistical-mechanics treatments of rubber elasticity, and ? and ? use statistical mechanics to analyze the mechanical systems of liquid-crystal elastomers.

(Note: Electrostatic response)

? and ?, among others, extensively examined the response of polymers to electrostatic excitation on the macroscopic and microscopic scales. They discussed and analyzed the constitutive relations for the macroscopic electric parameters, such as polarization and displacement, and for the microscopic electric parameters, such as the dipole moments and the bound and free charge densities. Moreover, in his analysis from a charge to a continuum, ? developed an electrostatic theory that treats rigid bodies as ideal theoretical constructs.

(Note: Coupled response)

? was the first to analyze the coupled electromechanical response of DEs at the macroscopic level. Years later, ? introduced the constitutive behavior of electro-sensitive elastomers via an invariant-based representation, following which ? expanded this approach to anisotropic materials. Among others, ? and ? investigated how deformation and the rate of deformation affected electromechanical coupling. At the macroscopic level, ? analyzed the electromechanical response of membranes under a uniaxial force, under equal-biaxial forces, and for a membrane constrained in one direction and subject to a force in the opposite direction. Additionally, they examined the response of a fiber-constrained membrane. ? presented a principle of virtual work for problems involving combined electrostatic and mechanical loading and that includes the interactions between the resulting strain and polarization. Physically motivated multiscale analyses of electromechanical coupling were done by ?, ?, and ?, and ? introduced multiscale analysis based on statistical mechanics.

(Note: Experimental work)

In addition to these theoretical works, the dielectric properties of DEs have been extensively investigated experimentally over the past two decades. For example, some report that the relative permittivity of DEs such as VHB 4910/4905 remains relatively constant under biaxial extension (see, e.g., ? and ?), although others have contradicted these conclusions. In addition, several investigations have revealed a decrease in the relative permittivity with increasing area stretch. For example, ? measured an initial relative permittivity $\epsilon_r = 4.4$ versus $\epsilon_r = 2.25$ for a ninefold area stretch, and ? measured $\epsilon_r = 4.68$ versus $\epsilon_r = 2.62$ for a 25-fold area stretch. In addition, ? measured an initial permittivity $\epsilon_r = 4.36$ versus $\epsilon_r = 2.44$ for a 16-fold planar stretch. ? found experimen-

tally from the electromechanical response of a polyurethane elastomer that chain motion can be divided into motion related to the mechanical response and motion related to the polarization response, and that the overlap between these motions yields the electromechanical response. Other experimental works, such as ?, ?, and ?, examined biaxially and uniaxially prestrained silicone and acrylic elastomers to study how prestraining DE membranes affects actuator performance. Finally, work has been done to developing models for estimating the variation in relative permittivity as a function of various stretch combinations [??]. An example of such work is was done by ?, who compared the results of a statistical-mechanics-based model with experimental findings.

(Note: This work)

(Note: A brief description of the displayed content)

We begin this work by discussing the theoretical background within the framework of a continuum approach and considering the mechanical, electrostatic, and coupled cases. Next, we review the analysis of the microstructure of an isotropic polymer chain network by using statistical mechanics with entropy considerations and make reference to a phenomenological model for the electromechanical coupling of DEs that will be tested against experimental results. Section 3 analyzes the DE electro-elasticity in several hierarchical cases, ranging from a single electric charge to a network. In addition, we discuss the means of assessing the structure and properties of a general polymer. Section 4 presents a numerical application of the electrostatically biased polymer network to demonstrate how polymerizing a polymer under an electric field affects the structure of the polymer network and its properties. This work is done by comparing the electric-field-polymerized polymer to an isotropic polymer network and to the results of the phenomenological model. Section 5 presents our experimental work, which gives an additional perspective on our theoretical work. The experimental work includes an evaluation of how uniaxial and biaxial stretching of DEs affects their dielectric constant. Moreover, we introduce a new experimental system that allows us to evaluate how the dielectric constant of DEs on the electric-field magnitude. Finally, the conclusions are gathered in Section 6.

2 Theoretical background

(Note: Multiscale entropy based analysis)

The mechanical and electrostatic energy balance is formulated in terms of the electric enthalpy. The analyses take into account the entropy of the chain network within the framework of statistical mechanics with the appropriate kinematic and energetic constraints.

2.1 Continuum electro-elasticity

(Note: basic continuum mechanics - mechanics aspect)

Consider an electro-elastic solid continuum in a stress-free configuration in the absence of electric field and mechanical load. Let material particles be labeled by their position vector \mathbf{X} in this referential configuration. In the deformed configuration, the point \mathbf{X} occupies the position $\mathbf{x} = \chi(\mathbf{X}, \mathbf{t})$, where the vector field χ describes the deformation of the material. We require χ to be a one-to-one, orientation-preserving, and twice continuously differentiable mapping [?].

(Note: continuum mechanics - mechanics)

The deformation gradient tensor is

$$\mathbf{F} = \nabla_{\mathbf{X}}\chi(\mathbf{X}, \mathbf{t}), \quad (1)$$

where $\nabla_{\mathbf{X}}$ is the gradient operator and the subscript \mathbf{X} implies that the derivatives are taken with respect to the referential coordinate system. The Cartesian components of \mathbf{F} are $F_{ij} = \frac{\partial \mathbf{x}_i}{\partial \mathbf{X}_j}$, where \mathbf{X}_i and \mathbf{x}_i ($i = 1, 2, 3$) are the Cartesian components of \mathbf{X} and \mathbf{x} , respectively. $J \equiv \det(\mathbf{F})$ is the ratio between volume elements in the current and reference configurations, with the convention of being strictly positive. Moreover, the velocity of the material points is $\mathbf{v}(\mathbf{x})$, the spatial velocity gradient is

$$\mathbf{L} = \nabla_{\mathbf{x}}\mathbf{v} = \dot{\mathbf{F}}\mathbf{F}^{-1}, \quad (2)$$

where $\nabla_{\mathbf{x}}$ is the gradient operator taken with respect to the current coordinate system.

(Note: continuum mechanics - electrostatic)

The body is subjected to an electric field $\mathbf{E}(\mathbf{x})$, which satisfies the relation $\nabla_{\mathbf{x}} \times \mathbf{E}(\mathbf{x}) = 0$ in the entire space. The electric potential ϕ is a scalar quantity defined such that $\mathbf{E} = -\nabla_{\mathbf{x}}\phi$. The electric induction, also known as the electric displacement, is

$$\mathbf{D}(\mathbf{x}) = \epsilon_0 \mathbf{E}(\mathbf{x}) + \mathbf{P}(\mathbf{x}), \quad (3)$$

where the constant ϵ_0 is the vacuum permittivity and $\mathbf{P}(\mathbf{x})$ is the electric-dipole density, also known as the polarization ($\mathbf{P} = 0$ in vacuum). The electric displacement in ideal dielectrics or in a continuum with no free charges is governed by

$$\nabla_{\mathbf{x}} \cdot \mathbf{D}(\mathbf{x}) = 0. \quad (4)$$

(Note: continuum mechanics - the electromechanical coupling)

The electrical boundary conditions for the electromechanical problem are given in terms of the electric potential or the charge per unit area ρ_a on the boundary, which is the charge on the electrodes such that $\mathbf{D} \cdot \hat{\mathbf{n}} = -\rho_a$, where $\hat{\mathbf{n}}$ is the outer-pointing unit vector normal to the boundary in the current configuration. The mechanical boundary conditions are stated in terms of the displacement or the mechanical traction \mathbf{t} . The electric field in the surrounding space induces a Maxwell stress

$$\boldsymbol{\sigma}^M = \epsilon_0 \left(\mathbf{E} \otimes \mathbf{E} - \frac{1}{2}(\mathbf{E} \cdot \mathbf{E})\mathbf{I} \right). \quad (5)$$

Accordingly, the traction boundary condition is $(\boldsymbol{\sigma} - \boldsymbol{\sigma}^M) \hat{\mathbf{n}} = \mathbf{t}$. Assuming no body forces, the stress that develops in a dielectric $\boldsymbol{\sigma}$ due to the electromechanical loading satisfy the equilibrium equation

$$\nabla_{\mathbf{x}} \cdot \boldsymbol{\sigma} = 0. \quad (6)$$

(Note: The first law of thermodynamics - energy balance)

The balance of energy is formulated by applying the first law of thermodynamics:

$$\frac{dU}{dt} = \frac{dW}{dt} + \frac{dQ}{dt}, \quad (7)$$

where U represents the internal energy stored in the material, W is the work done on the system by any external sources, mechanical or electrical, and Q is the energy supplied to the system as heat. Following ?? and ?, a Legendre transform is applied to the internal energy to formulate the energy balance in terms of the electric-enthalpy density: $H = U - J\mathbf{P} \cdot \mathbf{E}$. To formulate the energy balance in terms of entropy, which relates to the number of microscopic configurations of the system, we refer to a polymer as a reversible or conservative material [?] (i.e., a material that does not absorb the work done by external agents but stores it as dielectric polarization or elastic deformation). Thus, following the Clausius theorem for a reversible material or system, the entropy change is $dS = \frac{dQ}{T}$, where S is the entropy-density per unit referential volume and T is the absolute temperature. Thus, taking into account the analysis presented in appendix A [?], we

consider a general representation in which the first law of thermodynamics takes the form

$$\dot{H}^r - \frac{d}{dt} \int_{\mathbb{R}^3} \frac{\epsilon_0}{2} \mathbf{E} \cdot \mathbf{E} dV = \dot{W}^r + T \dot{S}^r, \quad (8)$$

where we consider an electro-elastic system $\mathcal{V} \subset \mathbb{R}^3$.

? gives the following specific representation of Eq. (8) to analyze the energy balance in a single polymer chain:

$$\frac{d}{dt} \int_{V_0} H(\mathbf{F}, \mathbf{E}) dV_0 - \frac{d}{dt} \int_{\mathbb{R}^3} \frac{\epsilon_0}{2} \mathbf{E} \cdot \mathbf{E} dV = \frac{dW}{dt} + T \frac{d}{dt} \int_{V_0} S(\mathbf{F}, \mathbf{E}) dV_0, \quad (9)$$

where, in the current configuration, we consider a dielectric body that occupies the region $V_0 \subset \mathbb{R}^3$ with a boundary ∂V_0 before the deformation and the region $V \subset \mathbb{R}^3$ with a boundary ∂V after the deformation.

The rate of change in electric enthalpy is [?]

$$\frac{d}{dt} \int_{V_0} H(\mathbf{F}, \mathbf{E}) dV_0 = \int_V \frac{1}{J} \frac{\partial H(\mathbf{F}, \mathbf{E})}{\partial \mathbf{F}} \mathbf{F}^T : \mathbf{L} dV + \int_V \frac{1}{J} \frac{\partial H(\mathbf{F}, \mathbf{E})}{\partial \mathbf{E}} \cdot \dot{\mathbf{E}} dV, \quad (10)$$

and the rate of change in entropy is

$$\frac{d}{dt} \int_{V_0} S(\mathbf{F}, \mathbf{E}) dV_0 = \int_V \frac{1}{J} \frac{\partial S(\mathbf{F}, \mathbf{E})}{\partial \mathbf{F}} \mathbf{F}^T : \mathbf{L} dV + \int_V \frac{1}{J} \frac{\partial S(\mathbf{F}, \mathbf{E})}{\partial \mathbf{E}} \cdot \dot{\mathbf{E}} dV. \quad (11)$$

If we assume no free charges in the material and neglect body forces, the power extracted by the external mechanical and electrical agents on the system is [???

$$\frac{dW}{dt} = \int_{\partial V} \mathbf{t} \cdot \mathbf{v} dA - \int_{\partial V} \rho_a \frac{d\phi}{dt} dA, \quad (12)$$

which can also be formulated as [?]

$$\frac{dW}{dt} = \int_V (\boldsymbol{\sigma} - \boldsymbol{\sigma}^M - \mathbf{E} \otimes \mathbf{P}) : \mathbf{L} dV - \frac{d}{dt} \int_{\mathbb{R}^3} \frac{\epsilon_0}{2} \mathbf{E} \cdot \mathbf{E} dV - \int_V \mathbf{P} \cdot \dot{\mathbf{E}} dV + \int_{\mathbb{R}^3/V} (\boldsymbol{\sigma} - \boldsymbol{\sigma}^M) : \mathbf{L} dV. \quad (13)$$

By using Eqs. (10), (11), and (13) in Eq. (9), we obtain

$$\begin{aligned} & \int_V \left(\frac{1}{J} \left(T \frac{\partial S(\mathbf{F}, \mathbf{E})}{\partial \mathbf{E}} - \frac{\partial H(\mathbf{F}, \mathbf{E})}{\partial \mathbf{E}} \right) - \mathbf{P} \right) \cdot \dot{\mathbf{E}} dV + \int_{\mathbb{R}^3/V} (\boldsymbol{\sigma} - \boldsymbol{\sigma}^M) : \mathbf{L} dV + \\ & \int_V \left(\boldsymbol{\sigma} - \boldsymbol{\sigma}^M - \mathbf{E} \otimes \mathbf{P} - \frac{1}{J} \left(\frac{\partial H(\mathbf{F}, \mathbf{E})}{\partial \mathbf{F}} - T \frac{\partial S(\mathbf{F}, \mathbf{E})}{\partial \mathbf{F}} \right) \mathbf{F}^T \right) : \mathbf{L} dV = 0. \end{aligned} \quad (14)$$

Because we have assumed that Eq. (14) fits every acceptable process, we can follow ? to

Figure 1: A schematic description of the coordinate system $\{\hat{\mathbf{E}}, \hat{\mathbf{Y}}, \hat{\mathbf{Z}}\}$ and the applied spherical coordinates.

obtain

$$\boldsymbol{\sigma} = \boldsymbol{\sigma}^m + \mathbf{E} \otimes \mathbf{P} + \boldsymbol{\sigma}^M, \quad (15)$$

where

$$\boldsymbol{\sigma}^m = \frac{1}{J} \left(\frac{\partial H(\mathbf{F}, \mathbf{E})}{\partial \mathbf{F}} - T \frac{\partial S(\mathbf{F}, \mathbf{E})}{\partial \mathbf{F}} \right) \mathbf{F}^T, \quad (16)$$

is the mechanical stress [?], and $\mathbf{E} \otimes \mathbf{P}$ is the polarization stress, with

$$\mathbf{P} = \frac{1}{J} \left(T \frac{\partial S(\mathbf{F}, \mathbf{E})}{\partial \mathbf{E}} - \frac{\partial H(\mathbf{F}, \mathbf{E})}{\partial \mathbf{E}} \right). \quad (17)$$

Furthermore, when dealing with incompressible materials,

$$\boldsymbol{\sigma} = \boldsymbol{\sigma}^m + \mathbf{E} \otimes \mathbf{P} + \boldsymbol{\sigma}^M + p_\star \mathbf{I}, \quad (18)$$

where p_\star is an arbitrary Lagrange multiplier corresponding to the indeterminate hydrostatic pressure that results from the incompressibility constraint and \mathbf{I} is the identity matrix. The corresponding deviatoric stress, which is related to shape change, is

$$\boldsymbol{\sigma}_{\text{Dev}} = \boldsymbol{\sigma} - \frac{\text{tr}(\boldsymbol{\sigma})}{3} \mathbf{I}. \quad (19)$$

2.2 Entropy-driven electro-elasticity of an isotropic polymer network

(Note: defining the construct and directions in the polymer)

The work of ? indicates that analyzing the properties and structure of different polymers starts with a single polymer chain with n dipolar monomers. Let l be the length between the two contact points of a monomer with its neighbors and define a coordinate system $\{\hat{\mathbf{E}}, \hat{\mathbf{Y}}, \hat{\mathbf{Z}}\}$ (Fig. 1) for a chain subjected to an electric field $\mathbf{E} = E\hat{\mathbf{E}}$. In this system,

$$\hat{\boldsymbol{\xi}} = \cos \theta \hat{\mathbf{E}} + \sin \theta (\cos \phi \hat{\mathbf{Y}} + \sin \phi \hat{\mathbf{Z}}) \quad (20)$$

is a unit vector where $0 \leq \theta < \pi$ is the angle between $\hat{\boldsymbol{\xi}}$ and the electric field and $0 \leq \phi < 2\pi$ is the angle of its projection onto the plane perpendicular to $\hat{\mathbf{E}}$ and $\hat{\mathbf{Y}}$. We define $d\Gamma = \sin \theta d\theta d\phi$ as the differential solid angle and allow Γ to vary from 0 to Γ_0 .

(**Note:** a chain's number of possible configurations and constraints (+Stirling's approximation))

The number of possible configurations of a single polymer chain is

$$\Omega^C = \frac{n!}{\prod_i (n_i!)}, \quad (21)$$

where n_i is the number of dipolar monomers aligned along $\hat{\xi}_i$ in the range $\theta_i \leq \theta < \theta_i + d\theta$ and $\phi_i \leq \phi < \phi_i + d\phi$. For convenience, we define that θ_i and ϕ_i correspond to the unit vector $\hat{\xi}_i$. The entropy of the chain is

$$S^C = k \ln(\Omega^C) = k \left(n \ln(n) - n - \sum_i n_i \ln(n_i) + \sum_i n_i \right), \quad (22)$$

where we have used Stirling's approximation and k is Boltzmann's constant. The chain is subjected to three constraints:

$$\sum_i n_i = n, \quad (23)$$

$$\sum_i l n_i \hat{\xi}_i = \mathbf{r}, \quad (24)$$

where the end-to-end vector of the monomer chain is $\mathbf{r} = r \hat{\mathbf{r}}$, with $\hat{\mathbf{r}} = \cos \Theta \hat{\mathbf{E}} + \sin \Theta (\cos \Phi \hat{\mathbf{Y}} + \sin \Phi \hat{\mathbf{Z}})$, and

$$\sum_i n_i h_i = H^C, \quad (25)$$

where h_i is the electric enthalpy of a monomer directed along $\hat{\xi}_i$ and H^C is the enthalpy of the chain.

(**Note:** maximizing the entropy according to the constraints)

We assume that the polymer chain occupies the most probable configuration under the given constraints, so we are interested in maximizing the entropy

$$S^C = k \left[\ln(\Omega^C) + \alpha \left(\sum_i n_i - n \right) + \boldsymbol{\tau} \cdot \left(\sum_i n_i \hat{\xi}_i - \frac{\mathbf{r}}{l} \right) + \gamma \left(\sum_i n_i h_i - H^C \right) \right], \quad (26)$$

where α , $\boldsymbol{\tau}$, and γ are Lagrange multipliers. The derivative of S_C with respect to n_i is

$$\frac{\partial S^C}{\partial n_i} = k \left[-\ln(n_i) + \alpha + \boldsymbol{\tau} \cdot \hat{\xi}_i + \gamma h_i \right] = 0, \quad (27)$$

from which

$$n_i = \exp \left(\alpha + \boldsymbol{\tau} \cdot \hat{\xi}_i + \gamma h_i \right). \quad (28)$$

Upon substitution of the latter into Eq. (26), the maximum entropy that can be achieved

by the chain is [?]

$$S^C = k \left[n \ln(n) - \alpha n - \boldsymbol{\tau} \cdot \frac{\mathbf{r}}{l} - \gamma H^C \right]. \quad (29)$$

(Note: Lagrange multiplier - inverse temperature)

We assume that the polymer chains do not interact with one another. Consequently, in a volume element dV_0 , the total entropy density and the total electrical-enthalpy density are $S = \frac{1}{dV_0} \sum_k S_k^C$ and $H = \frac{1}{dV_0} \sum_k H_k^C$, respectively. Applying the first law of thermodynamics with respect to the enthalpy of the k -th chain, we obtain

$$\frac{\partial H}{\partial H_k^C} = T \frac{\partial S}{\partial H_k^C}, \quad (30)$$

from which we derive the relation

$$\gamma = -\frac{1}{kT} \quad (31)$$

with the help of Eq. (29).

(Note: PDF of a monomer according to the constraints and with maximum entropy (+calculating the rest of the Lagrange multipliers and Hc))

From the constraints (23) and (27), we obtain

$$\sum_i n_i = \exp(\alpha) \int_0^{r_0} \exp\left(\boldsymbol{\tau} \cdot \hat{\boldsymbol{\xi}} - \frac{h}{kT}\right) d\Gamma = n, \quad (32)$$

where Eq. (29) is used and the summation is replaced by an integral over all monomer orientations. Therefore,

$$\exp(\alpha) = \frac{n}{Z}, \quad (33)$$

where

$$Z = \int_0^{r_0} \exp\left(\boldsymbol{\tau} \cdot \hat{\boldsymbol{\xi}} - \frac{h}{kT}\right) d\Gamma, \quad (34)$$

is the partition function. Subsequently, Eq. (28) we have that

$$p(\hat{\boldsymbol{\xi}}, h) = \frac{1}{Z} \exp\left(\boldsymbol{\tau} \cdot \hat{\boldsymbol{\xi}} - \frac{h}{kT}\right) \quad (35)$$

is the probability density function (PDF) that a monomer is aligned in the direction $\hat{\boldsymbol{\xi}}$ and has an electrical enthalpy h . An implicit equation that gives the Lagrange multiplier $\boldsymbol{\tau}$ follows from constraint (24):

$$\int_0^{r_0} \hat{\boldsymbol{\xi}} p d\Gamma = \frac{\mathbf{r}}{nl}. \quad (36)$$

From Eq. (25) the enthalpy of the chain is

$$\int_0^{r_0} h p d\Gamma = H^C. \quad (37)$$

(Note: monomer enthalpy and different dipole types)

Following ??? and ?, the electric enthalpy of a dipole oriented along $\hat{\xi}$ is

$$h = \mathbf{m} \cdot \mathbf{E}, \quad (38)$$

where the dipole vector \mathbf{m} is determined according to a relevant model that represents the local relation. We account for three specific models, the first of which corresponds to a spontaneous dipole or a rigid dipole with constant magnitude [?]

$$\mathbf{m}_S = \kappa_P \hat{\xi}. \quad (39)$$

The second model is of a uniaxial dipole whose magnitude depends on the electric field [?]:

$$\mathbf{m}_U = \kappa_U \hat{\xi} \otimes \hat{\xi} \mathbf{E}, \quad (40)$$

where κ_U is commonly referred to as the *polarizability* of the dipole. The third type is the transversely isotropic (TI) model [?]:

$$\mathbf{m}_{TI} = \frac{1}{2} \kappa_{TI} (\mathbf{I} - \hat{\xi} \otimes \hat{\xi}) \mathbf{E}, \quad (41)$$

where the dipole is perpendicular to $\hat{\xi}$. Note that we do not account for the local electrostatic interactions between the dipolar monomers, so a uniform electric field is induced over the monomers in the chain.

For three dielectrics composed of a random and uniform distribution of spontaneous, uniaxial, and transversely isotropic dipoles to behave the same in the limit of infinitesimal deformations and small electric fields, we impose $\kappa_U = \kappa_{TI} = \frac{\kappa_P^2}{kT} = \kappa$. The polarizability is $\kappa = \frac{3}{n_0} \epsilon_0 \chi_0$ [?], where $\chi_0 = \epsilon_r - 1$ is the initial susceptibility and ϵ_r is the relative permittivity. $n_0 = N n$ is the number of monomers in a unit referential volume where N is the number of chains in the unit referential volume.

(Note: PDF in the amorphous case)

For an amorphous polymer, the chain's constraints, given by Eqs. (23), (24), and (25), are irrelevant because no such limitations exist for a single monomer. Therefore, $\tau = 0$

and the adjusted form of the PDF in Eq. (35) is

$$p(\hat{\boldsymbol{\xi}}) = \frac{1}{Z} \exp\left(-\frac{h}{kT}\right), \quad (42)$$

where

$$Z = \int \exp\left(-\frac{h}{kT}\right) d\Gamma, \quad (43)$$

and the enthalpy of the monomer is calculated by using Eq. (38) with the correct dipole type.

(Note: analytical calculation - PDF in the amorphous case - U and TI)

In addition to the numerical calculations for the PDF in the amorphous case, the amorphous monomer distribution can also be calculated by applying the analytical analysis of ?, giving

$$p_U = \frac{\omega}{4\pi D(\omega)} \exp\left[-\omega^2 \sin^2(\theta_i)\right] \quad (44)$$

as the PDF of the uniaxial dipole, where $\omega = \sqrt{\frac{\kappa}{kT}} E = \frac{\kappa_P E}{kT}$ and $D(\omega) = \exp(-\omega^2) \int_0^\omega \exp(t^2) dt$ is the Dawson function. The PDF for the TI dipole is

$$p_{TI} = \frac{\omega}{(2\pi)^{3/2} \text{Erf}\left(\frac{\omega}{\sqrt{2}}\right)} \exp\left[-\frac{\omega^2}{2} \cos^2(\theta_i)\right], \quad (45)$$

where $\text{Erf}(x)$ is the error function.

2.3 Phenomenological approach to electro-elasticity

(Note: A reference for the results in the application section)

We compare the results of the theory developed above with those of a relatively simple phenomenological predictive material model that uses reasonable assumptions and is based on continuum mechanics. In the current work, a constitutive law for the material must be expressed through an energy-density function that depends on both the deformation and the electric displacement or the electric field. Thus, as a reference, we recall the extended neo-Hookean energy-density function for an ideal elastic dielectric (IED) [?]:

$$W(\mathbf{F}, \mathbf{E}) = \frac{\mu}{2} \left[\text{Tr}(\mathbf{F}^T \mathbf{F} - \mathbf{I}) \right] + \frac{\epsilon_0 \epsilon_r}{2} \mathbf{E} \cdot \mathbf{E}, \quad (46)$$

where μ is the shear modulus of the material. From Eq. (46) and assuming conservation of energy and a reversible or conservative material, the constitutive equations for an

incompressible IED can be expressed as

$$\boldsymbol{\sigma} = \mathbf{F} \frac{\partial W}{\partial \mathbf{F}} + p_{\star} \mathbf{I} = \mu \mathbf{F} \mathbf{F}^{\text{T}} + \mathbf{E} \otimes \mathbf{D} + p_{\star} \mathbf{I}, \quad (47)$$

and

$$\mathbf{D} = \epsilon_0 \epsilon_r \mathbf{E}, \quad (48)$$

in accordance with Eq. (3) with the relative permittivity considered to be constant. Note that, in general, this model does not accurately reproduce experimental results for coupled electromechanical loading.

Figure 2: Schematic description of an arbitrary one dimensional system subjected to electromechanical excitation at its boundary.

3 Electro-elasticity of solutions and anisotropic networks of polymer molecules

We now present an in-depth multiscale analysis of the electromechanical coupling in DEs based on their inherent microstructure. This analysis allows us to examine the interplay between the macroscopic deformation of DEs and the rearrangement of the monomers in a network of polymer chains as a result of external electrical and mechanical loading.

3.1 First law of thermodynamics

The first law of thermodynamics, expressed in Eq. (8), is formulated as a general representation of the electromechanical situation. This representation accounts for the conservation of energy in a body subjected to an electric field while allowing us to formulate the energy balance in terms of the electric enthalpy and the entropy of the system.

To systematically analyze the electromechanical coupling in polymers from the microscopic to the macroscopic level, we tailor Eq. (8) to five different systems. The simplest systems are based on that presented in Fig. 2, which is essentially a one-dimensional system. Subsequently, we examine a network that is treated as a three-dimensional body.

3.2 One-dimensional systems of charges, dipoles, and molecular chains in an electric field

In a one-dimensional system (see Fig. 2), we define the vector connecting the two ends (i.e., the end-to-end vector of the system) as $\mathbf{r} = \mathbf{r}_- - \mathbf{r}_+$. The quantities $\mathbf{f}^{+/-}$, $\mathbf{V}^{+/-}$, and $Q^{+/-}$ are the forces, velocities, and charges, respectively, at the system boundaries. The rate of change in enthalpy and in entropy are $\dot{H}^r = \dot{H}(\mathbf{r}, \mathbf{E}_0)$ and $\dot{S}^r = \dot{S}(\mathbf{r}, \mathbf{E}_0)$, respectively. The power extracted by the external agents [see Eq. (12)] is $\dot{W}^r = \sum \mathbf{f} \cdot \mathbf{V} + \sum Q \dot{\phi}$.

Figure 3: Schematic description of a single charge subjected to an electric field.

3.2.1 A single electric charge

We begin by analyzing the second term of Eq. (8), which concerns the variation in the energy of the system due to variations in the electric field generated by a single charge. To be precise, the present case describes a zero-dimensional system.

The electric field due to a particle with a constant electric charge Q is derived from Coulomb's law as

$$\mathbf{E}^Q(\mathbf{g}) = \frac{Q\hat{\mathbf{g}}}{4\pi\epsilon_0 g^2}, \quad (49)$$

where in the current case $\mathbf{g} = g\hat{\mathbf{g}}$ is the vector from a specific point in space to the charge's location. Thus, because electric fields satisfy the superposition principle, the total electric field at the given location is

$$\mathbf{E}(\mathbf{g}) = \mathbf{E}_0 + \mathbf{E}^Q(\mathbf{g}) = \mathbf{E}_0 + \frac{Q\hat{\mathbf{g}}}{4\pi\epsilon_0 g^2}, \quad (50)$$

where $\mathbf{E}_0 = E_0 \hat{\mathbf{E}}$ is the electric field imposed on the entire space. Accordingly, the second term in Eq. (8) is

$$\begin{aligned} & \frac{\epsilon_0}{2} \frac{d}{dt} \int_{\mathbb{R}^3} \left(\mathbf{E}_0 \cdot \mathbf{E}_0 + 2 \frac{Q\mathbf{E}_0 \cdot \hat{\mathbf{g}}}{4\pi\epsilon_0 g^2} + \frac{Q\hat{\mathbf{g}}}{4\pi\epsilon_0 g^2} \cdot \frac{Q\hat{\mathbf{g}}}{4\pi\epsilon_0 g^2} \right) dV \\ &= \frac{\epsilon_0}{2} \frac{d}{dt} \int_{\mathbb{R}^3} \left(\mathbf{E}_0 \cdot \mathbf{E}_0 + \frac{Q\mathbf{E}_0 \cdot \hat{\mathbf{g}}}{2\pi\epsilon_0 g^2} + \frac{Q^2}{16\pi^2 \epsilon_0^2 g^4} \right) dV. \end{aligned} \quad (51)$$

Note that the first and third terms in Eq. (51) are constants. Moreover, for any spherical region about a charge with inner radius R_i and outer radius R_o , the variation in the energy depends on

$$\frac{Q}{4\pi} \int_0^{2\pi} \int_0^\pi \int_{R_i}^{R_o} \frac{\mathbf{E}_0 \cdot \hat{\mathbf{g}}}{g^2} g^2 \sin \Theta dg d\Theta d\Phi = \frac{QE_0}{2} \frac{d}{dt} \int_{R_i}^{R_o} dg \int_0^\pi \cos \Theta \sin \Theta d\Theta \equiv 0, \quad (52)$$

where $\mathbf{E}_0 \cdot \hat{\mathbf{g}} = E_0 \cos \Theta$ [Eq. (20)]. Since this integral vanishes identically, so does its time derivative. Thus, for any motion of a single charge in a uniform electric field, the second term in Eq. (8) vanishes.

Taking into account Eq. (52) and neglecting the enthalpy and entropy since we assume no material, Eq. (8) is reduced to $\dot{W} = 0$. Thus, based on Fig. 3 and Eq. (12), we obtain

Figure 4: Schematic description of a single dipole consisting of two charges, Q^+ and Q^- , connected by a stiff rod in an electric field.

for a single charge

$$\dot{W} = \mathbf{f} \cdot \frac{d\mathbf{c}}{dt} - Q \frac{d\phi}{dt} = 0, \quad (53)$$

where \mathbf{c} gives the location of the charge. The velocity of the charge is $\mathbf{V} = \frac{d\mathbf{c}}{dt}$ where $d\mathbf{c} = \delta\hat{\mathbf{E}} + d\mathbf{c}_T$ represents the change in position of the charge during the time interval dt , $d\phi = -\mathbf{E}_0 \cdot d\mathbf{c} = -\delta E_0$, and $\mathbf{f} = f_E \hat{\mathbf{E}} + \mathbf{f}_T$. Moreover, $d\mathbf{c}_T$ and \mathbf{f}_T are the components of $d\mathbf{c}$ and \mathbf{f} , respectively, that are perpendicular to the direction $\hat{\mathbf{E}}$. Thus,

$$\dot{W} = \frac{d}{dt} (\mathbf{f} \cdot d\mathbf{c} + Q\delta E_0) = \frac{d}{dt} (f_E \delta + \mathbf{f}_T \cdot d\mathbf{c}_T + Q\delta E_0) = 0. \quad (54)$$

Therefore, because Eq. (54) equals zero in an equilibrium state and $d\mathbf{c}_T$ is arbitrary, we conclude that $\mathbf{f}_T \equiv 0$ and $f_E = -QE_0$. This is precisely Coulomb's force on a charge of magnitude Q in an electric field \mathbf{E}_0 .

3.2.2 Dipoles

Consider now a charged nonpolarized rigid dipole and, as in the previous case, assume no material and neglect the enthalpy and entropy. As indicated in Fig. 4, the dipole consists of two charges Q^+ and Q^- connected by a stiff rod of length l oriented in the direction of the unit vector $\hat{\boldsymbol{\xi}}$. We assume that $Q^+ = -Q^- = Q$.

Again, we begin by analyzing the second term in Eq. (8), which gives the variation in system energy due to variations in the electric field generated by the charges. Thus, in accordance with the superposition principle,

$$\begin{aligned} \mathbf{E} &= \mathbf{E}_0 + \mathbf{E}^{Q^+}(\mathbf{g}^+) - \mathbf{E}^{Q^-}(\mathbf{g}^-) = \mathbf{E}_0 + \frac{Q\hat{\mathbf{g}}^+}{4\pi\epsilon_0(g^+)^2} - \frac{Q\hat{\mathbf{g}}^-}{4\pi\epsilon_0(g^-)^2} \\ &= \mathbf{E}_0 + \mathbf{E}^+ + \mathbf{E}^-, \end{aligned} \quad (55)$$

where $\mathbf{g}^+ = g^+\hat{\mathbf{g}}^+$ and $\mathbf{g}^- = g^-\hat{\mathbf{g}}^-$ are vectors from a specific point in space to the positions of charges Q^+ and Q^- , respectively. Accordingly, the second term in Eq. (8) is

$$\frac{\epsilon_0}{2} \frac{d}{dt} \int_{\mathbb{R}^3} \left(\mathbf{E}_0 \cdot \mathbf{E}_0 + 2(\mathbf{E}_0 \cdot \mathbf{E}^+ + \mathbf{E}_0 \cdot \mathbf{E}^- + \mathbf{E}^+ \cdot \mathbf{E}^-) + \mathbf{E}^+ \cdot \mathbf{E}^+ + \mathbf{E}^- \cdot \mathbf{E}^- \right) dV, \quad (56)$$

Figure 5: Schematic description of a dipole in an electric field.

where, according to Eq. (52), the integrals over $\mathbf{E}_0 \cdot \mathbf{E}^+$ and $\mathbf{E}_0 \cdot \mathbf{E}^-$ vanishes identically and the remaining terms are constant. Thus, Eq. (56) equals zero.

As a result, Eq. (8) again reduces to $\dot{W} = 0$. From the definition of electric potential, $d\phi = -\mathbf{E}_0 \cdot d\mathbf{c}$, so $\dot{\phi}^{+/-} = -\mathbf{E}_0 \cdot \mathbf{V}^{+/-}$ and the rate of work of the external sources is

$$\dot{W} = \mathbf{f}^+ \cdot \mathbf{V}^+ + \mathbf{f}^- \cdot \mathbf{V}^- + \mathbf{E}_0 \cdot (Q^+ \mathbf{V}^+ + Q^- \mathbf{V}^-) = 0. \quad (57)$$

Since $\mathbf{c}^+ = \mathbf{c}^- + l\hat{\boldsymbol{\xi}}$ from the geometry of the situation, then $\mathbf{V}^+ = \mathbf{V}^- + l\dot{\hat{\boldsymbol{\xi}}}$ and the corresponding rate of work is

$$\dot{W} = (\mathbf{f}^+ + \mathbf{f}^-) \cdot \mathbf{V}^- + l(\mathbf{f}^+ + Q\mathbf{E}_0) \cdot \dot{\hat{\boldsymbol{\xi}}} = 0. \quad (58)$$

Because the dipole is rigid, it is constrained along the direction of the dipole. Thus, the forces and the electric field may be split into components in the orthogonal system $\{\hat{\boldsymbol{\xi}}, \hat{\mathbf{u}}, \hat{\mathbf{s}}\}$, where $\hat{\mathbf{s}} = \hat{\boldsymbol{\xi}} \times \hat{\mathbf{E}}$ is perpendicular to the plane spanned by the electric field and the dipole. $\hat{\mathbf{u}} = \hat{\mathbf{s}} \times \hat{\boldsymbol{\xi}}$ is perpendicular to the dipole and is on the given plane. Using $\mathbf{f}^+ = a^+\hat{\boldsymbol{\xi}} + b^+\hat{\mathbf{u}} + c^+\hat{\mathbf{s}}$, $\mathbf{f}^- = a^-\hat{\boldsymbol{\xi}} + b^-\hat{\mathbf{u}} + c^-\hat{\mathbf{s}}$, and $\mathbf{E}_0 = e\hat{\boldsymbol{\xi}} + g\hat{\mathbf{u}}$, Eq. (58) yields

$$\dot{W} = [(a^+ + a^-)\hat{\boldsymbol{\xi}} + (b^+ + b^-)\hat{\mathbf{u}} + (c^+ + c^-)\hat{\mathbf{s}}] \cdot \mathbf{V}^- + l[a^+\hat{\boldsymbol{\xi}} + b^+\hat{\mathbf{u}} + c^+\hat{\mathbf{s}} + Q(e\hat{\boldsymbol{\xi}} + g\hat{\mathbf{u}})] \cdot \dot{\hat{\boldsymbol{\xi}}} = 0. \quad (59)$$

Since Eq. (59) equals zero at equilibrium and \mathbf{V}^- and $\dot{\hat{\boldsymbol{\xi}}}$ are arbitrary, the first term implies that $a^+ = -a^-$, $b^+ = -b^-$, and $c^+ = -c^-$. However, consideration of the second term shows that $c^+ = 0$. Moreover, since $\dot{\hat{\boldsymbol{\xi}}} \perp \hat{\boldsymbol{\xi}}$, the dot product of the component oriented along the dipole with the temporal derivative of the dipole vanishes identically. Thus, the second term of Eq. (59) does not constrain the components of the forces in the dipole direction and $b^+ = -gQ$. These results are analogous to the requirement that the sum of the dipole moments vanishes.

For spontaneous and polarizable dipolar monomers (Fig. 5), the electric enthalpy must be taken into account. According to ?, the electric enthalpy of a dipole is

$$h = -\mathbf{m} \cdot \mathbf{E}_0, \quad (60)$$

where \mathbf{m} is the dipole vector. For a spontaneous dipole with constant magnitude κ , $\mathbf{m} = \kappa\hat{\boldsymbol{\xi}}$. Thus, the electric enthalpy is $h = -\kappa\hat{\boldsymbol{\xi}} \cdot \mathbf{E}_0$ and the rate of change of electric enthalpy

is

$$\dot{h} = -\kappa \dot{\hat{\boldsymbol{\xi}}} \cdot \mathbf{E}_0. \quad (61)$$

In this, case Eq. (8) reduces to

$$\dot{h} = \dot{W}. \quad (62)$$

Substituting Eqs. (58) and (61) into Eq. (62) yields

$$-\kappa \dot{\hat{\boldsymbol{\xi}}} \cdot \mathbf{E}_0 = \mathbf{f}^+ \cdot \mathbf{V}^+ + \mathbf{f}^- \cdot \mathbf{V}^- = (\mathbf{f}^+ + \mathbf{f}^-) \cdot \mathbf{V}^- + l \mathbf{f}^+ \cdot \dot{\hat{\boldsymbol{\xi}}}, \quad (63)$$

which leads to

$$(\mathbf{f}^+ + \mathbf{f}^-) \cdot \mathbf{V}^- + (l \mathbf{f}^+ + \kappa \mathbf{E}_0) \cdot \dot{\hat{\boldsymbol{\xi}}} = 0. \quad (64)$$

Again, the forces and the electric field are split into components in the orthogonal system $\{\hat{\boldsymbol{\xi}}, \hat{\mathbf{u}}, \hat{\mathbf{s}}\}$, where $\mathbf{f}^+ = a^+ \hat{\boldsymbol{\xi}} + b^+ \hat{\mathbf{u}} + c^+ \hat{\mathbf{s}}$, $\mathbf{f}^- = a^- \hat{\boldsymbol{\xi}} + b^- \hat{\mathbf{u}} + c^- \hat{\mathbf{s}}$, and $\mathbf{E}_0 = e \hat{\boldsymbol{\xi}} + g \hat{\mathbf{u}}$. Accordingly, Eq. (58) yields

$$\left[(a^+ + a^-) \hat{\boldsymbol{\xi}} + (b^+ + b^-) \hat{\mathbf{u}} + (c^+ + c^-) \hat{\mathbf{s}} \right] \cdot \mathbf{V}^- + \left[l (a^+ \hat{\boldsymbol{\xi}} + b^+ \hat{\mathbf{u}} + c^+ \hat{\mathbf{s}}) + \kappa (e \hat{\boldsymbol{\xi}} + g \hat{\mathbf{u}}) \right] \cdot \dot{\hat{\boldsymbol{\xi}}} = 0. \quad (65)$$

Given that \mathbf{V}^- and $\dot{\hat{\boldsymbol{\xi}}}$ are arbitrary, the first term leads to the constraints $a^+ = -a^-$, $b^+ = -b^-$, and $c^+ = -c^-$. The second term leads to $c^+ = 0$ and, given that $\dot{\hat{\boldsymbol{\xi}}} \perp \hat{\boldsymbol{\xi}}$, the second term contributes no additional constraint on the components of the forces in the dipole direction and $b^+ = -g \frac{\kappa}{l}$. If $b^+ = 0$ then $\mathbf{E}_0 \cdot \dot{\hat{\boldsymbol{\xi}}} = 0$ for equilibrium and, because $\dot{\hat{\boldsymbol{\xi}}} \perp \hat{\boldsymbol{\xi}}$, we have $\hat{\boldsymbol{\xi}} \parallel \mathbf{E}_0$ for this specific case, which means that the electric field causes no rotation of the dipole, so the dipole remains at rest in the absence of external forces.

3.2.3 Polymer molecule (chain)

As established above, when $\frac{d}{dt} \int_{\mathbb{R}^3} \mathbf{E} \cdot \mathbf{E} dV$ vanishes identically and $\dot{W} = 0$, Eq. (8) reduces to

$$\dot{H} = T \dot{S}. \quad (66)$$

Thus, because $T \dot{S}^C - \dot{H}^C = 0$ describes an equilibrium state for a polymer chain, the preferred state of a chain may be described by determining $\max \{T S^C - H^C\}$. Then, taking Eq. (29) into account, the most probable state is the one that satisfies

$$\max \left\{ T k \left[n \ln(n) - \alpha n - \boldsymbol{\tau} \cdot \frac{\mathbf{r}}{l} \right] - (T k \gamma + 1) H^C \right\}, \quad (67)$$

where Eq. (25) gives $H^C(\mathbf{r}, \mathbf{E}_0) = \sum_{i=1}^n h_i(\hat{\boldsymbol{\xi}}_i, \mathbf{E}_0)$. Note that the analysis assumes that r , the end-to-end length of the chain with maximum permutations (i.e., the most probable

length), is the only end-to-end length of chains in the direction $\hat{\mathbf{r}}$.

(Note: The "length" of a polymer chain - general)

To determine the most probable length r for a specific chain, the number of possible permutations is calculated for all possible end-to-end lengths in the range $0 \leq r \leq nl$. This assessment is done for chains in all possible orientations relative to the direction of the electric field, $0 \leq \Theta < \pi$. Thus, we can assess the most probable chain configuration, depending on the magnitude of the electric field in the polymerization process and the chain's inclination with respect to the electric field.

(Note: The "length" of a polymer chain in the case of $E=0$ - purely mechanical case)

When examining the vector \mathbf{r} of a single polymer chain when $\mathbf{E}_0 = 0$, then $H^C(\mathbf{r}, 0) = 0$ and the entropy of the chain governs its behavior. By using the implicit equation from which the Lagrange multiplier $\boldsymbol{\tau}$ is computed and the PDF that a monomer is in the direction $\hat{\boldsymbol{\xi}}$, Eqs. (36) and (35), respectively, we obtain

$$\frac{\int_0^{r_0} \hat{\boldsymbol{\xi}} \exp(\boldsymbol{\tau} \cdot \hat{\boldsymbol{\xi}}) d\Gamma}{\int_0^{r_0} \exp(\boldsymbol{\tau} \cdot \hat{\boldsymbol{\xi}}) d\Gamma} = \frac{\mathbf{r}}{nl}. \quad (68)$$

Let $\boldsymbol{\tau} = a\hat{\mathbf{r}} + b\hat{\mathbf{m}}$, where $\hat{\mathbf{m}} = \frac{\mathbf{m}}{m}$ and $\mathbf{m} = \boldsymbol{\tau} - (\boldsymbol{\tau} \cdot \hat{\mathbf{r}})\hat{\mathbf{r}}$ in an orthogonal system $\{\hat{\mathbf{r}}, \hat{\mathbf{m}}, \hat{\mathbf{s}}\}$ where $\hat{\mathbf{s}} = \hat{\mathbf{r}} \times \hat{\mathbf{m}}$. In this system, define $\hat{\boldsymbol{\xi}} = \cos \theta \hat{\mathbf{r}} + \sin \theta (\cos \phi \hat{\mathbf{m}} + \sin \phi \hat{\mathbf{s}})$, which leads to $\boldsymbol{\tau} \cdot \hat{\boldsymbol{\xi}} = a \cos \theta + b \sin \theta \cos \phi$.

Multiplying Eq. (68) by $\hat{\mathbf{m}}$ gives

$$\frac{1}{Z} \int_0^{r_0} (\hat{\boldsymbol{\xi}} \cdot \hat{\mathbf{m}}) \exp(\boldsymbol{\tau} \cdot \hat{\boldsymbol{\xi}}) d\Gamma = 0, \quad (69)$$

or

$$\frac{1}{Z} \int_0^{2\pi} \int_0^\pi \exp(a \cos \theta) \exp(b \sin \theta \cos \phi) \sin \theta \cos \phi (\sin \theta d\theta d\phi) = 0. \quad (70)$$

Note that the choice $b = 0$ leads to

$$\frac{1}{Z} \int_0^\pi \exp(a \cos \theta) \sin^2 \theta d\theta \int_0^{2\pi} \cos \phi d\phi = 0, \quad (71)$$

which fulfills Eq. (69).

Multiplying the left-hand side of Eq. (68) by $\hat{\mathbf{r}}$ gives

$$\frac{1}{Z} \int_0^{r_0} (\hat{\boldsymbol{\xi}} \cdot \hat{\mathbf{r}}) \exp(\boldsymbol{\tau} \cdot \hat{\boldsymbol{\xi}}) d\Gamma = \frac{1}{Z} \int_0^{2\pi} \int_0^\pi \exp(a \cos \theta) \cos \theta \sin \theta d\theta d\phi. \quad (72)$$

A change of variables to $x = \cos \theta$ leads to

$$\frac{\int_{-1}^1 \exp(ax) x dx}{\int_{-1}^1 \exp(ax) dx} = \frac{r}{nl}, \quad (73)$$

which can be integrated to obtain

$$\frac{\exp(a) + \exp(-a)}{\exp(a) - \exp(-a)} - \frac{1}{a} \equiv \mathcal{L}(a) = \frac{r}{nl}, \quad (74)$$

where \mathcal{L} is the Langevin function. Accordingly,

$$a = \mathcal{L}^{-1}\left(\frac{r}{nl}\right), \quad (75)$$

where \mathcal{L}^{-1} is the inverse Langevin function. Note that if $\frac{r}{nl} \ll 1$ then $a \cong \frac{3r}{nl}$ and $a \rightarrow \infty$ in the limit $r \rightarrow nl$.

Substituting the expression for S^C following Eqs. (22) and (26) gives

$$\begin{aligned} \ln(\Omega^C) &= n \ln(n) - \sum_i n_i \ln(n_i) \\ &= n \left\{ \ln(n) - \frac{1}{Z} \left[\ln\left(\frac{n}{Z}\right) \int_0^{r_0} \exp(a \cos \theta) d\Gamma + a \int_0^{r_0} \exp(a \cos \theta) \cos \theta d\Gamma \right] \right\}, \end{aligned} \quad (76)$$

where, from Eq. (72),

$$\int_0^{r_0} \exp(a \cos \theta) \cos \theta d\Gamma = \frac{r}{nl} \int_0^{r_0} \exp(a \cos \theta) d\Gamma, \quad (77)$$

so

$$\begin{aligned} \ln(\Omega^C) &= n \left\{ \ln(n) - \frac{1}{Z} \left[\left(\ln\left(\frac{n}{Z}\right) + \frac{ar}{nl} \right) \int_0^{r_0} \exp(a \cos \theta) d\Gamma \right] \right\} \\ &= n \ln(Z) - a \frac{r}{l}. \end{aligned} \quad (78)$$

Note that

$$Z = \frac{2\pi}{a} [\exp(a) - \exp(-a)], \quad (79)$$

so

$$\ln(\Omega^C) = n \ln \left\{ \frac{2\pi}{a} [\exp(a) - \exp(-a)] \right\} - a \frac{r}{l}. \quad (80)$$

Note also that, in the limit $r \rightarrow 0$, $\ln(\Omega^S) = n \ln(4\pi)$ so $\Omega^S = (4\pi)^n$ and, in the limit $r \rightarrow nl$, $\ln(\Omega^{nl}) = n \ln \left[\frac{2\pi}{a} \exp(a) \right] - an = n \ln \left(\frac{2\pi}{a} \right)$ so $\Omega^{nl} = \left(\frac{2\pi}{a} \right)^n \rightarrow 0$ since $a \rightarrow \infty$.

Given that $\mathbf{E}_0 = 0$, the total number of permutations of chains with end-to-end length r is

$$\Omega^O(r) = 4\pi r^2 \Omega^C(r) = 4\pi n^2 l^2 \eta^2 \Omega^C, \quad (81)$$

where $\eta \equiv \frac{r}{nl}$. In the limit $r \rightarrow 0$, Ω^S is finite and $\Omega^O(0) \rightarrow 0$, and in the limit $r \rightarrow nl$, $\Omega^S \rightarrow 0$ and r^2 is finite, so $\Omega^O(nl) \rightarrow 0$. This suggests that, in the range $0 < r < nl$, Ω^O has a maximum.

The maximum of Ω^O is obtained by using

$$\frac{d \ln \Omega^C}{d\eta} = \frac{\partial \ln \Omega^C}{\partial a} \frac{da}{d\eta} + \frac{\partial \ln \Omega^C}{\partial \eta}, \quad (82)$$

where we treat a and η as independent variables. Equations (74) and (80) show that

$$\begin{aligned} \frac{\partial \ln \Omega^C}{\partial a} &= n \left(\frac{\exp(a) + \exp(-a)}{\exp(a) - \exp(-a)} - \frac{1}{a} \right) - \frac{r}{l} \\ &= n \left(\frac{\exp(a) + \exp(-a)}{\exp(a) - \exp(-a)} - \frac{1}{a} \right) - n\eta = 0, \end{aligned} \quad (83)$$

so

$$\frac{d \ln \Omega^C}{d\eta} = -a n. \quad (84)$$

From the distribution for the case $\mathbf{E}_0 = 0$ [see Eq. (81)] and using $4\pi n^2 l^2 = k$, we obtain

$$\frac{1}{k} \frac{\partial \Omega^O}{\partial \eta} = 2\eta \Omega^C + \eta^2 \frac{d\Omega^C}{d\eta} = \eta \exp(\ln \Omega^C) [2 - \eta a n] = 0. \quad (85)$$

Therefore $a = \frac{2}{n\eta}$ or $\eta = \mathcal{L}\left(\frac{2}{n\eta}\right) = \coth\left(\frac{2}{n\eta}\right) - \frac{n\eta}{2}$. For large n , $\coth\left(\frac{2}{n\eta}\right) = \frac{n\eta}{2} + \frac{2}{3n\eta} + o\left(\frac{2}{n\eta}\right)^3$. Thus, up to a second order in $\frac{1}{n}$, $\eta = \sqrt{\frac{2}{3}} \frac{1}{\sqrt{n}} \sim \frac{0.816}{\sqrt{n}}$. This result differs from the assessment obtained from random walk statistics presented and used by ??? and ? but is consistent with the assessed end-to-end chain length determined by ? , ? , and ? .

(Note: force in a single chain with no electric field)

Furthermore, assuming zero electric field, we examine the most probable end-to-end length of a chain subjected to a force $\mathbf{f} \parallel \mathbf{r}$ and with one end at the origin and the other located within a small volume $dV = r^2 dr d\phi d\theta$. For a single chain with no electric field, Eq. (8) takes the form

$$\dot{W} + T \dot{S}^O(\mathbf{r}) = 0. \quad (86)$$

For this case, we define $\mathbf{r} = \rho \mathbf{R}$, where ρ is the stretch magnitude \mathbf{R} is the end-to-end vector in the referential state of the chain, and we assume that $\mathbf{r} \parallel \mathbf{R}$. Thus, in accordance

with Eqs. (22) and (81), the rate of change of entropy is

$$\dot{S}^O(\mathbf{r}) = \frac{dS^O}{d\rho} \dot{\rho} = k \left(\frac{2}{\rho} - \frac{\boldsymbol{\tau} \cdot \mathbf{R}}{l} \right) \dot{\rho}, \quad (87)$$

and the rate of work done by the external sources is

$$\dot{W} = \mathbf{f} \cdot \mathbf{v} = \mathbf{f} \cdot \mathbf{R} \dot{\rho}, \quad (88)$$

where $\mathbf{v} = \dot{\mathbf{r}}$, \mathbf{f} is the external force exerted on the chain, and body forces are neglected. Substituting Eqs. (87) and (88) into Eq. (86) yields

$$\begin{aligned} \left[\mathbf{f} \cdot \mathbf{R} + T k \left(\frac{2}{\rho} - \frac{\boldsymbol{\tau} \cdot \mathbf{R}}{l} \right) \right] \dot{\rho} &= \left[\mathbf{f} \cdot \mathbf{R} \rho + T k \left(2 - \frac{\boldsymbol{\tau} \cdot \mathbf{R} \rho}{l} \right) \right] \dot{\rho} \\ &= [\mathbf{f} \cdot \mathbf{r} + T k (2 - \eta \tau n)] \dot{\rho} = 0, \end{aligned} \quad (89)$$

thus,

$$\mathbf{f} = -\frac{T k (2 - \eta \tau n)}{r^2} \mathbf{r} = -\frac{T k \left[2 - \frac{r}{nl} \mathcal{L}^{-1} \left(\frac{r}{nl} \right) n \right]}{r} \hat{\mathbf{r}}, \quad (90)$$

where Eq. (75) is taken into account. Thus, in accordance with Eq. (85), when $\frac{r}{nl} = \sqrt{\frac{2}{3}} \frac{1}{\sqrt{n}}$ then $\mathbf{f} = 0$.

3.3 Polymer molecules (chains) in electric field

We now examine a method for controlling the electro-elastic moduli of a network. Specifically, we examine the consequence of polymerization in an external electric field. Toward this end, we assume that the polymer chains are in solution during the polymerization and that the monomers are already bonded into chains but that the chains are not cured and toughened or hardened into a network by cross-linking. In this case, we refer to the chains as “floating” in the solution such that no external work is applied at their ends. Furthermore, we assume no interactions between the chains and determine their most probable permutations separately.

Given these assumptions, each chain is examined individually. The end-to-end length of a chain is $r_j = r(\Theta_j, \mathbf{E}_0)$ and the end-to-end direction of a chain is $\hat{\mathbf{r}}_j = \hat{\mathbf{r}}(\Theta_j, \Phi_j)$. In the coordinate system shown in Fig. 1, Θ_j is the inclination of the chains’ end-to-end vector relative to the direction of the electric field. Thus, as described in section 3.2.3, the suitable r_j for each Θ_j is the one that satisfies Eq. (67). When $E = 0$, only a single chain need be analyzed (as detailed in Sec. 3.2.3) because the polymer has no preferred direction in this case and the network is isotropic.

3.3.1 Distribution of monomer orientation

(Note: calculating monomer orientations)

After calculating the polymer end-to-end chain length in each group, we evaluate the orientation of the chain building blocks (i.e., the monomers). The monomer orientations are investigated as a part of a chain while taking into account the suitable constraints, as indicated by Eqs. (23)–(25).

Once the end-to-end chain lengths are determined for the maximum possible permutations (i.e., the most probable end-to-end chain length for each group), the monomer distribution is calculated for each chain by using Eq. (35). The probabilities for all possible monomer orientations are then calculated to determine the monomer distribution in the most probable chain, which was obtained in the previous section. These orientations include all combinations in the ranges $0 \leq \theta < \pi$ and $0 \leq \phi < 2\pi$.

After obtaining the monomer orientations for each chain group, we compare it with the monomer distribution in the amorphous phase, which can be calculated by using Eq. (42) and taking into account the correct type of dipole. Analytical approximations of the PDF in the amorphous phase are given by Eqs. (44) and (45) for uniaxial dipoles and transversely isotropic dipoles, respectively [?].

3.4 An anisotropic network of polymer molecules

According to ?, the total number of internal configurations of a polymer with N polymer chains is

$$\Omega^t = N! \prod_q \left(\frac{(\omega_q)^{N_q}}{N_q!} \right), \quad (91)$$

where ω_q and N_q are the number of configurations and the number of chains associated with a specific end-to-end vector, respectively. As an example, assume that we can *a priori* split the chain population into two populations such that, for all the end-to-end vectors in the two groups, the numbers of possible configurations are ω_1 and ω_2 and the numbers of chains in each group are N_1 and N_2 , respectively. The total end-to-end vectors ψ_1 and ψ_2 in the two groups satisfy $\psi_1 N_1 + \psi_2 N_2 = N$. Accordingly,

$$\Omega^t = N! \left(\prod_{q_1=1}^{\psi_1} \frac{(\omega_1)^{N_1}}{N_1!} \right) \left(\prod_{q_2=1}^{\psi_2} \frac{(\omega_2)^{N_2}}{N_2!} \right) = N! \left(\frac{(\omega_1)^{N_1}}{N_1!} \right)^{\psi_1} \left(\frac{(\omega_2)^{N_2}}{N_2!} \right)^{\psi_2}. \quad (92)$$

Similarly, given J groups with a similar number of configurations and of chains in each group,

$$\Omega^t = N! \prod_{j=1}^J \left(\frac{(\omega_j)^{N_j}}{N_j!} \right)^{\psi_j}, \quad (93)$$

where ψ_j is the number of end-to-end vectors in group j group and

$$\sum_j \psi_j N_j = N. \quad (94)$$

The number of possible configurations of a polymer chain is

$$\omega_j = \frac{n_j!}{\prod_i (n_{ij}!)}, \quad (95)$$

where n_j is the number of dipolar monomers in a chain in group j and n_{ij} is the number of monomers aligned with $\hat{\xi}_i$ in a chain in group j . Consequently, by using the Stirling approximation, the total entropy of the polymer is

$$\begin{aligned} S^t &= k \ln(\Omega^t) \\ &= k \left(N \ln(N) - N + \sum_j \psi_j \left\{ N_j \left[n_j \ln(n_j) - n_j - \sum_i n_{ij} \ln(n_{ij}) + \sum_i n_{ij} \right] - N_j \ln(N_j) + N_j \right\} \right) \\ &= k \left\{ N \ln(N) + \sum_j \psi_j N_j \left[n_j \ln(n_j) - \sum_i n_{ij} \ln(n_{ij}) - \ln(N_j) \right] \right\}. \end{aligned} \quad (96)$$

The polymer network is subjected to the constraint mentioned in Eq. (94). As previously specified, each chain is subject to three constraints:

$$\sum_i n_{ij} = n_j, \quad (97)$$

$$\sum_i n_{ij} \hat{\xi}_i = \mathbf{r}_j, \quad (98)$$

and the end-to-end vector of the monomer chain is $\mathbf{r}_j = r_j \hat{\mathbf{r}}_j$, so

$$\sum_i n_{ij} h_i = H_j^C, \quad (99)$$

where H_j^C is the electric enthalpy of the chain and h_i is the enthalpy of a monomer aligned along $\hat{\xi}_i$.

We assume that the most probable configuration is the configuration currently occupied by the polymer, so we are interested in maximizing the entropy under the given

constraints:

$$S^t = k \ln(\Omega_t) + k \sum_j \psi_j N_j \left[\alpha_j \left(\sum_i n_{ij} - n_j \right) + \boldsymbol{\tau}_j \cdot \left(\sum_i n_{ij} \hat{\boldsymbol{\xi}}_i - \frac{\mathbf{r}_j}{l} \right) + \gamma_j \left(\sum_i n_{ij} h_i - H_j^C \right) \right] + k \eta \left(\sum_j \psi_j N_j - N \right), \quad (100)$$

where α_j , $\boldsymbol{\tau}_j$, γ_j , and η are Lagrange multipliers.

To account for the maximal number of configurations, we impose

$$\frac{\partial S^t}{\partial n_{ij}} = k \left[-\psi_j N_j \ln(n_{ij}) + \psi_j N_j \left(\alpha_j + \boldsymbol{\tau}_j \cdot \hat{\boldsymbol{\xi}}_i + \gamma_j h_i \right) \right] = 0, \quad (101)$$

from which we obtain

$$n_{ij} = \exp \left(\frac{\psi_j N_j \left(\alpha_j + \boldsymbol{\tau}_j \cdot \hat{\boldsymbol{\xi}}_i + \gamma_j h_i \right)}{\psi_j N_j} \right) = \exp \left(\alpha_j + \boldsymbol{\tau}_j \cdot \hat{\boldsymbol{\xi}}_i + \gamma_j h_i \right). \quad (102)$$

By substituting Eq. (101) into Eq. (100), the maximum entropy of the polymer is

$$S^t = k N \ln(N) + k \sum_j \psi_j \{ N_j [n_j \ln(n_j)] - N_j \ln(N_j) \} - \sum_j \psi_j N_j \left(\alpha_j n_j + \boldsymbol{\tau}_j \cdot \frac{\mathbf{r}_j}{l} + \gamma_j H_j^C \right) + k \eta \left(\sum_j \psi_j N_j - N \right). \quad (103)$$

Following the works of ? and ?, we also assume no interaction between the polymer chains. Therefore, the total enthalpy is $H_t = \sum_j \psi_j N_j H_j^C$. Differentiating the first law of thermodynamics [Eq. (8)] with respect to the enthalpy of the j th we have that

$$\frac{\partial H^t}{\partial H_j^C} = T \frac{\partial S^t}{\partial H_j^C}, \quad (104)$$

and by using Eq. (103), we obtain

$$\gamma_j = -\frac{1}{kT}. \quad (105)$$

By taking into consideration the constraint imposed by Eq. (97) and the relations given by Eqs. (102) and (105), we obtain

$$\sum_i n_{ij} = \int_0^{\Gamma_0} \exp \left(\alpha_j + \boldsymbol{\tau}_j \cdot \hat{\boldsymbol{\xi}}_i - \frac{h_i}{kT} \right) d\Gamma = n_j. \quad (106)$$

From here we can determine the PDF, which indicates that a monomer in chain j is

oriented along $\hat{\xi}_i$ and has an electric enthalpy h_i . This is

$$p_{ij}(\hat{\xi}_i, h_i) = \frac{n_{ij}}{n_j} = \frac{1}{Z_j} \exp\left(\tau_j \cdot \hat{\xi}_i - \frac{h_i}{kT}\right), \quad (107)$$

where

$$Z_j = \int_0^{\Gamma_0} \exp\left(\tau_j \cdot \hat{\xi}_i - \frac{h_i}{kT}\right) d\Gamma, \quad (108)$$

is the partition function and the Lagrange multipliers τ_j are computed from the implicit equations that follow from the constraints given by Eq. (98),

$$\int_0^{\Gamma_0} \hat{\xi}_i p_{ij} d\Gamma = \frac{\mathbf{r}_j}{n_j l}. \quad (109)$$

The enthalpy of the chain,

$$\int_0^{\Gamma_0} h_i p_{ij} d\Gamma = H_j^C, \quad (110)$$

is computed from constraint given by Eq. (99).

To consider the network with the largest number of chain configurations, we impose that

$$\begin{aligned} \frac{\partial S^t}{\partial N_j} &= \psi_j \left[n_j \ln(n_j) - \sum_i n_{ij} \ln(n_{ij}) - \ln(N_j) \right] + \psi_j \alpha_j \left(\sum_i n_{ij} - n_j \right) + \psi_j \tau_j \cdot \left(\sum_i n_{ij} \hat{\xi}_i - \frac{\mathbf{r}_j}{l} \right) \\ &\quad + \psi_j \gamma_j \left(\sum_i n_{ij} h_i - H_j^C \right) + \eta \psi_j \\ &= \psi_j \left[n_j \ln(n_j) - \sum_i n_{ij} \ln(n_{ij}) - \ln(N_j) + \eta \right] = 0, \end{aligned} \quad (111)$$

from which we obtain

$$N_j = \exp \left[n_j \ln(n_j) - \sum_i n_{ij} \ln(n_{ij}) + \eta \right] = \frac{\exp(\eta) n_j^{n_j}}{\prod_i n_{ij}^{n_{ij}}}. \quad (112)$$

Next, from the constraint given by Eq. (94), we obtain

$$\sum_j \psi_j N_j = \sum_j \psi_j \frac{\exp(\eta) n_j^{n_j}}{\prod_i n_{ij}^{n_{ij}}} = N. \quad (113)$$

This enables us to determine the Lagrange multiplier

$$\eta = \ln \left(\frac{N}{\sum_j \left(\frac{\psi_j n_j^{n_j}}{\prod_i n_{ij}^{n_{ij}}} \right)} \right). \quad (114)$$

Furthermore, the PDF that a chain is in the j -th inclination is

$$p_j = \frac{N_j}{N} = \frac{\prod_i n_{ij}^{-n_{ij}}}{\sum_k \psi_k \prod_i n_{ik}^{-n_{ik}}} = \frac{\prod_i (n_j p_{ij})^{-n_j p_{ij}}}{\sum_k \psi_k \prod_i (n_k p_{ik})^{-n_k p_{ik}}}, \quad (115)$$

and the fraction of all the chains with a specific inclination to the electric field can be estimated as

$$v_j = \psi_j p_j, \quad (116)$$

such that $\sum_j v_j = 1$.

Next, we use Eq. (115) in Eq. (103) to determine the entropy of the entire network:

$$\begin{aligned} S^t &= k \left\{ N \ln(N) + \sum_j \psi_j N_j \left[n_j \ln(n_j) - \sum_i n_{ij} \ln(n_{ij}) - \ln \left(N \frac{\prod_i n_{ij}^{-n_{ij}}}{\sum_k \psi_k \prod_i n_{ik}^{-n_{ik}}} \right) \right] \right\} \\ &= k N \ln(N) + k \sum_j \psi_j N_j \left[n_j \ln(n_j) - \sum_i n_{ij} \ln(n_{ij}) - \ln(N) \right] \\ &\quad + k \sum_j \psi_j N_j \left[\sum_i n_{ij} \ln(n_{ij}) + \ln \left(\sum_k \psi_k \prod_i n_{ik}^{-n_{ik}} \right) \right] \\ &= k \left\{ \sum_j \psi_j N_j \left[n_j \ln(n_j) + \ln \left(\sum_k \psi_k \prod_i n_{ik}^{-n_{ik}} \right) \right] \right\}. \end{aligned} \quad (117)$$

Assuming a fixed number of dipolar monomers in each chain, we neglect the first term in the last line of Eq. (117) to conclude that

$$S^t \propto N \ln \left(\sum_k \psi_k \prod_i n_{ik}^{-n_{ik}} \right). \quad (118)$$

By following the same steps for the case of the entropy of a chain presented in Eq. (22), we conclude that

$$S_j^C \propto \ln \left(\prod_i n_{ij}^{-n_{ij}} \right). \quad (119)$$

Similarities appear between both assessments of the maximum entropy. In Eq. (119), the entropy of a chain is a function of the end-to-end length r_j and does not depend on the inclination $\hat{\mathbf{r}}$.

Note that, for excitation by an electric field, the number of end-to-end vectors in

group j depends on the group's inclinations with respect to the direction of the electric field, so

$$\psi_j = 2\pi r_j^2 \sin(\Theta_j). \quad (120)$$

3.4.1 Deriving the properties of the polymer

To assess our methodology, we evaluate the properties of a new anisotropic polymer and to compare them with those of an isotropic polymer. Besides the electromechanical coupling, which is our main interest, the response of the polymer to purely mechanical loading and electrostatic excitation is also examined. The mechanical properties of the polymer relate to the mechanical stress in the polymer under purely mechanical loading described by the deformation gradient tensor \mathbf{F} . The electrical properties of the polymer, such as the electric displacement and susceptibility, relate to the polarization of the polymer under electrostatic excitation.

(Note: referenced mechanical stress)

The general mechanical stress presented by ?, which results from Eq. (16), is

$$\boldsymbol{\sigma}^m = \frac{1}{J \text{dV}_0} \sum_i \left[n \left(\int_0^{r_0} \frac{\partial h}{\partial \mathbf{F}} p \text{d}\Gamma \right)_i + \frac{k T \boldsymbol{\tau}_i}{l} \frac{\partial \mathbf{r}_i}{\partial \mathbf{F}} \right] \mathbf{F}^T. \quad (121)$$

The mechanical stress takes into account the change in the electrical energy of the monomers due to the mechanical deformation and the mechanical loadings that deform the end-to-end vectors of the chains. As per ?, we assume that the monomer is rigid compared with the polymer chain, so the electric enthalpy of the monomer does not depend on the deformation gradient. Furthermore, by assuming an incompressible material, Eq. (121) simplifies to

$$\boldsymbol{\sigma}^m = \frac{1}{\text{dV}_0} \sum_i \left(\frac{k T \boldsymbol{\tau}_i}{l} \frac{\partial \mathbf{r}_i}{\partial \mathbf{F}} \right) \mathbf{F}^T. \quad (122)$$

(Note: simplified mechanical stress, suitable for an anisotropic case)

To determine the mechanical stress in the polymer, we first calculate the average stress of each chain group. As already mentioned, for excitation by an electric field, the chain groups are determined by their inclination with respect to the electric field. Thus, the stresses of chains with the same inclination Θ_k are averaged over $0 \leq \Phi_q < 2\pi$ to obtain

$$\boldsymbol{\sigma}_k^m = \frac{\sum_q^Q \left(\frac{k T \boldsymbol{\tau}_{kq}}{l} \frac{\partial \mathbf{r}_{kq}}{\partial \mathbf{F}} \right) \mathbf{F}^T}{Q}, \quad (123)$$

where $\hat{\mathbf{r}}_{kq} = \cos \Theta_k \hat{\mathbf{E}} + \sin \Theta_k (\cos \Phi_q \hat{\mathbf{Y}} + \sin \Phi_q \hat{\mathbf{Z}})$, and $q = 1, 2, \dots, Q$. The calculation of $\frac{\partial \mathbf{r}_{kq}}{\partial \mathbf{F}}$ is detailed in Appendix B.

Next, we consider the relative influence of each chain group by taking into account the fraction of chains in a specific group, as shown in Eq. (116). Thus, Eq. (122) can be rewritten as

$$\boldsymbol{\sigma}^m = N \sum_k v_k \boldsymbol{\sigma}_k^m, \quad (124)$$

where the averaged stress of a chain is multiplied by the number N of chains per unit volume.

(Note: referenced polarization)

The polarization

$$\mathbf{P} = -\frac{1}{J dV_0} \sum_i \left[n \left(\int_0^{\Gamma_0} \frac{\partial h}{\partial \mathbf{E}} p d\Gamma \right)_i + \frac{k T \boldsymbol{\tau}_i}{l} \frac{\partial \mathbf{r}_i}{\partial \mathbf{E}} \right], \quad (125)$$

was derived by ? and stems from Eq. (17). The polarization equation (125) considers the variation in electric enthalpy of the monomers as a result of excitation by the electric field and the reorientation of the chains as a response to the electrical excitation. From the assumption that the chains undergo affine deformation follows that the electric field does not directly affect the chain distribution. Thus, by assuming an incompressible material, Eq. (125) simplifies to

$$\mathbf{P} = -\frac{n}{dV_0} \sum_i \left(\int_0^{\Gamma_0} \frac{\partial h}{\partial \mathbf{E}} p d\Gamma \right)_i. \quad (126)$$

(Note: simplified polarization, suitable for an anisotropic case + susceptibility)

The polarization of the polymer is calculated in the same way as for the mechanical stress. Because $\frac{\partial h}{\partial \mathbf{E}} = -\mathbf{m}$, the polarization of chains of a given inclination Θ_k are averaged over $0 \leq \Phi_q < 2\pi$ to obtain

$$\mathbf{P}_k = \frac{n \sum_q^Q \left(\int_0^{\Gamma_0} \mathbf{m} p d\Gamma \right)_{kq}}{Q}, \quad (127)$$

where $q = 1, 2, \dots, Q$.

Thus, because the relative influence of each chain group is considered through the fraction of chains in a specific group, we obtain

$$\mathbf{P} = N \sum_k v_k \mathbf{P}_k, \quad (128)$$

where the averaged polarization of a chain is multiplied by the number N of chains per unit

volume. After calculating the polarization, the electric displacement may be calculated by using Eq. (3), and the susceptibility can be calculated by using

$$\chi = \frac{\mathbf{P} \cdot \mathbf{E}}{\epsilon_0 E^2}. \quad (129)$$

4 Application to electrostatically biased network

(Note: Opening sentence + Isotropic example - first step of the numerical analysis - evaluating the Lagrange multiplier τ)

To modify DE properties to modify the electromechanical coupling of polymers, we propose to polymerize monomers in the presence of an external electric field. Such a process produces a relative order of the polymer-chain networks as the chains and dipolar monomers react to the electric field while the chains are forming and “floating” in solution. The electric field is removed after the polymer-chain network hardens as a result of cross-linking between chains. Note that the chain and monomer responses are restricted by the constraints (94) and (97)–(99), as detailed in Sec. 3.4.

To examine the influence of the proposed polymerization process (i.e., creating a “biased” polymer), we follow the analytical analysis detailed in Sec. 3. This examination is done while comparing the results for the biased polymer with those of an unbiased polymer (i.e., an isotropic polymer) and with the IED model (presented in Sec. 2.3), all to evaluate how the suggested process affects the structure and properties of the polymer.

4.1 Chain distribution

The initial step of the analysis is to determine the most probable configuration of the polymer chains of the isotropic and biased polymers. We first apply our calculation to the case of no electric field and for a network of isotropic chains. The initial step of the calculation is to determine the Lagrange multiplier τ by applying the Newton—Raphson method to Eq. (36). The first guess, τ_0 , is obtained by analytically estimating the Lagrange multiplier as a function of \mathbf{r} in a case where the electric field approaches zero,

$$\tau_0 = \frac{3\mathbf{r}}{nl}, \quad (130)$$

which is accurate in this specific case, as detailed in Appendix C.

(Note: chains length - isotropic distribution)

Given the maximum-entropy assumption and the fact that, in this case, there is no electric actuation or any other external influence, we assume an isotropic distribution of chains, which means that we can assess the end-to-end length of a chain in a single direction and relate it to all directions. Thus, to determine the most probable end-to-end chain length, the number of configurations of a chain with a specific \mathbf{r} is calculated and then multiplied by the surface area of a sphere with the same r , which represents the chains groups in the isotropic case, as discussed in Sec. 3.2.3 and shown by Eq. (81). The entropy for each case is calculated by using the result of Eq. (81) in Eq. (22). Several examples are presented in Fig. 6, which shows the entropy as a function of the normalized

Figure 6: The entropy of a polymer chain with uniaxial dipoles as a function of the normalized radius as $0 \leq \frac{r}{nl} \leq 1$ and $l = 100 \mu\text{m}$. The red continuous curve with circular markers corresponds to $n = 50$ and the brown curve with squares to $n = 100$. The dashed columns corresponds to the normalized radii in accordance with the results in section 3.2.3, $\frac{r}{nl} = \sqrt{\frac{2}{3}} \frac{1}{\sqrt{n}}$, and the dot-dashed columns to the results from random walk statistics, $\frac{r}{nl} = \frac{1}{\sqrt{n}}$.

radius $\frac{r}{nl}$ for $n = 50$ and $n = 100$ with $l = 100 \mu\text{m}$. The initial susceptibility used in these examples is $\chi_0 = 37$, which is about ten times the electric susceptibility of the commercially available polymer VHB 4910, and the analyses are done for the case of uniaxial dipoles. The difference between the curves in Fig. 6 is attributed to Eqs. (21), (22), and (81). Accordingly, the entropy of the chain increases with the number of monomers in the chain.

(Note: defining calculation parameters - material properties and calculations boundaries)

We assume a shear modulus $\mu = 10^5 \text{ Pa}$ for the polymer in its initial unloaded configuration. The number N of chains per unit volume is deduced from $\mu = N k T$ [??]. The normalized radii that correspond to the maximum points of the two curves in Fig. 6 are $\left(\frac{r}{nl}\right)_{n=50} \cong 0.1$ and $\left(\frac{r}{nl}\right)_{n=100} \cong 0.075$ and are consistent with the analytical predictions $\left(\frac{r}{nl}\right)_{n=50} = 0.115$ and $\left(\frac{r}{nl}\right)_{n=100} = 0.082$, respectively, given in Sec. 3.2.3 and shown by the dashed columns in Fig. 6. The difference between the numerical and analytical results for the most probable end-to-end chain length is associated with the density of discretization of 0.025 for $0 \leq \frac{r}{nl} \leq 1$. Furthermore, the results of the current approach differ from the results $\left(\frac{r}{nl}\right)_{n=50} = 0.141$ and $\left(\frac{r}{nl}\right)_{n=100} = 0.1$, obtained from the random walk statistics and presented by the dot-dashed columns in Fig. 6. Negative entropy is irrational and is truncated because it represents configurations that are incompatible with the assumption required for Stirling's approximation that is applied to go from Eq. (21) to Eq. (22).

(Note: the main idea - parameters value and initial calculations)

Next, to determine how electrical excitation affects the polymer structure during polymerization, different parameters were investigated as the electric-field magnitude ranged from $0 \frac{\text{MV}}{\text{m}}$ to $150 \frac{\text{MV}}{\text{m}}$. The results are based on a numerical calculation where the number of monomers in a single chain, the length between the two contact points of a monomer with its neighbors, and the number of chains per unit volume are the same as those assumed for the case of no electric field.

To demonstrate how electric fields of various magnitudes affect chains at various inclinations with respect to the electric field, Figs. 7, 8, and 9 show results for chains with $\Theta = \frac{\pi}{1000}$, $\Theta = \frac{\pi}{4}$ and $\Theta = \frac{\pi}{2}$. Figure 7 shows the natural logarithm of the maximum

pics for experimental work 16.1.2020/LnOmega vs ElecField

Figure 7: The natural logarithm for the maximum number of configurations as a function of the electric field magnitude for chains with uniaxial dipoles at different inclinations. The blue curve with circular markers corresponds to $\Theta = \frac{\pi}{1000}$, the red curve with squares to $\Theta = \frac{\pi}{4}$ and the yellow curve with diamonds to $\Theta = \frac{\pi}{2}$.

pics for experimental work 16.1.2020/rad vs ElecField 29.

Figure 8: The most probable end-to-end length as a function of the electric field magnitude for chains with uniaxial dipoles at different inclinations. The blue curve with circular markers corresponds to $\Theta = \frac{\pi}{1000}$, the red curve with squares to $\Theta = \frac{\pi}{4}$ and the yellow curve with diamonds to $\Theta = \frac{\pi}{2}$.

number of configurations for each chain as a function of electric field, and Fig. 8 shows the end-to-end length for the maximum number of configurations of each chain as a function of electric field. The Lagrange multiplier τ , which may be understood as the chain's mechanical constraint and which is related to the end-to-end length of the chain with the maximum number of configurations, is examined as a function of electric-field magnitude, as seen in Fig. 9.

Note from Figs. 7, 8, and 9 that the results differ little for an electric field less than $50 \frac{\text{MV}}{\text{m}}$. This is particularly evident in Fig. 8, where the change in the end-to-end length of the different chains is hardly visible below $50 \frac{\text{MV}}{\text{m}}$. Figure 7 shows the similarities in the curves for the natural logarithm of the maximum number of configurations for chains at different inclinations, which all decrease with increasing electric field. The differences between the curves attributed to the number of end-to-end vectors in each inclination with respect to the electric field, as expected from Eq. (120). Figure 8 shows that, with increasing electric field, the end-to-end length of chains at all inclinations increases. However, as the electric field increases, the differences in end-to-end length become more

pics for experimental work 16.1.2020/AbsTau vs ElecField

Figure 9: The size of the Lagrange multiplier τ , associated with the most probable radius as a function of the electric field magnitude for chains with uniaxial dipoles at different inclinations. The blue curve with circular markers corresponds to $\Theta = \frac{\pi}{1000}$, the red curve with squares to $\Theta = \frac{\pi}{4}$ and the yellow curve with diamonds to $\Theta = \frac{\pi}{2}$.

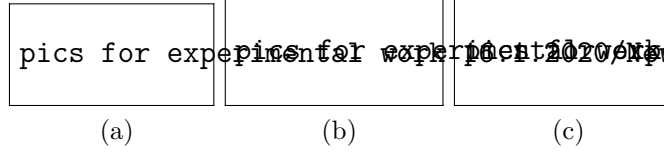


Figure 10: The monomer distribution for a polymer chain of uniaxial dipoles. The magnitude of the electric field during the polymerization process is $E = 150 \frac{\text{MV}}{\text{m}}$. (a) Corresponds to the chain with the inclination $\Theta = \frac{\pi}{1000}$ and end-to-end length $r = 0.89 \sqrt{n}l$. (b) Corresponds to $\Theta = \frac{\pi}{4}$ and $r = 0.91 \sqrt{n}l$. (c) Corresponds to $\Theta = \frac{\pi}{2}$ and $r = 0.93 \sqrt{n}l$.

prominent because chains at greater inclinations are longer. This result is counterintuitive because we would expect chains with greater inclination with respect to the electric field to be shorter because the monomers tend to reorient in the direction of the electric field. Figure 9 shows the difference in mechanical constraint of the chains. With increasing electric field, the constraint decreases for chains parallel to the electric field and increases somewhat for chains at greater inclinations. This result is attributed to the polymer being in a solution state during polymerization, and more energy is required to maintain chains at larger inclinations as the monomers react to the electric excitation.

4.2 Monomer orientation

(Note: monomer distribution - chains)

After calculating the end-to-end length for chains as a function of inclination with respect to the electric field [i.e., determining $\mathbf{r}_j^0 = r^0(\Theta_j, \mathbf{E})\hat{\mathbf{r}}(\Theta_j)$], the monomer orientation can be calculated as detailed in Sec. 3.3.1. Figures 10a(a)–10a(c) show the monomer distribution for chains with inclinations $\Theta = \frac{\pi}{1000}$, $\Theta = \frac{\pi}{4}$, and $\Theta = \frac{\pi}{2}$, respectively, and for an electric field $E = 150 \frac{\text{MV}}{\text{m}}$. In these three-dimensional plots, the length of the radius vector to each point represents the number of monomers aligned with the given vector. In addition, the monomer distribution is consistent when comparing different inclinations, which means that the monomers in the different chains tend to orient similarly. This consistency is very interesting because the chains have different inclinations and different end-to-end lengths.

(Note: amorphous monomer distribution)

Given that the monomer orientation for each given chain is obtained and their similarity is recognized, we now examine the monomer distribution in the amorphous case. Figure 11 presents the results of numerical calculations of the distribution of amorphous monomers distribution for a uniaxial dipole based on Eq. (42). Unlike Figs. 10a–10c, Fig. 11 presents a symmetric distribution of monomers, as in this case where monomers are free to reorient separately and not be constrained as part of a chain. The result of

Figure 11: The amorphous monomer distribution of a uniaxial dipole as $E = 150 \frac{\text{MV}}{\text{m}}$. According to the numerical analysis as $\tau = 0$ and identical to the results of the analytical analysis that was presented by ?.

Figure 12: The number of chains along each inclination as a function of the inclination relative to the direction of the electric field, $N(\Theta, \Phi = 0)$. The blue curve with circular markers corresponds to the isotropic polymer and the yellow curve with squares corresponds to the biased polymer.

the analytical analysis of the PDF in the amorphous case [?], presented in Eq. (44), also appears in Fig. 11 and are identical to the numerical results.

4.3 The free state

(Note: finding the natural state - chains distribution, weights and lambda0 deformation)

After analyzing the micro-scale and understanding the monomer distribution as a result of the given polymerization process, we now examine the macroscale. The analysis of the macroscopic response of polymers to different excitations, as detailed in Sec. 3.4, requires an assessment of the relative influence of each chain group in various inclinations. This assessment is done by using Eqs. (116) and (120) to calculate the fraction of chains with inclination j with respect to the electric field. Figure 12 compares the number of chains of various inclinations with respect to the electric field for isotropic polymers and electric-field-biased polymers, and Fig. 13 compares the fraction of chains in each inclination for each case. The relations between the results shown in Figs. 12 and 13 are credited to ψ_j , which is the number of end-to-end vectors in group j , as given by Eq. (120).

Figure 12 shows that the application of an external electric field during polymerization affects the chain distribution, as the chains aspire to align in the direction of the electric field. However, Fig. 13 shows that, because of Eq. (120), the most influential inclination of the polymer is $\Theta \cong \frac{\pi}{4}$.

To calculate the inclinations with respect to the direction of the electric field, the density of discretization was taken as $\Delta\Theta = \frac{\pi}{16}$ because denser discretizations do not significantly change the results. We refer to each individual group of chains in accordance with their inclinations with respect to the electric field, and we attribute each chain in

Figure 13: The fractions of chains along each inclination as a function of the inclination to the direction of the electric field, $\nu(\Theta)$. The blue curve with circular markers corresponds to the isotropic polymer and the yellow curve with squares corresponds to the biased polymer.

each group one end at the origin and the other end in a small volume $dV = r^2 dr d\phi d\theta$. Furthermore, because the DE coupling is quadratic in applied electric potential [?], the different DE responses can be deduced by analyzing $0 \leq \Theta \leq \frac{\pi}{2}$. Accordingly, the groups that relate to inclinations $\Theta = 0$ and $\Theta = \frac{\pi}{2}$, which are the boundaries of the analyzed range, are attributed to small volumes with $\Delta\Theta = \frac{\pi}{32}$. This is done to avoid exceeding the limits set for the angular range being tested.

Figure 14 presents the analysis of the deformation λ_0 of a polymer with respect to the electric field, induced during polymerization by the electric-field magnitude, given that the electric field is removed at the end of polymerization. The chains are unable to tune their length to that of the chains in the isotropic polymer because they are cross-linked and cannot rearrange separately. Thus, each chain is affected by the same deformation gradient. The corresponding deformation gradient, while assuming incompressibility, is

$$\mathbf{F}^0(\lambda_0) = \lambda_0 \hat{\mathbf{E}} \otimes \hat{\mathbf{E}} + \frac{1}{\sqrt{\lambda_0}} (\mathbf{I} - \hat{\mathbf{E}} \otimes \hat{\mathbf{E}}) = \begin{pmatrix} \lambda_0 & 0 & 0 \\ 0 & 1/\sqrt{\lambda_0} & 0 \\ 0 & 0 & 1/\sqrt{\lambda_0} \end{pmatrix}. \quad (131)$$

To assess the stress-free configuration of an incompressible body such as the biased polymer, we examine various deformation gradients. A suitable one is obtained from the state where $\boldsymbol{\sigma}_{EE} = \boldsymbol{\sigma}_{YY} = \boldsymbol{\sigma}_{ZZ} = \frac{\text{Tr}(\boldsymbol{\sigma})}{3}$ because the deviatoric stress is zero, in accordance with Eq. (19). As seen in Fig. 14, λ_0 is achieved by calculating $\boldsymbol{\sigma}_{EE} - \boldsymbol{\sigma}_{YY} = \boldsymbol{\sigma}_{\text{Diff}}$ and determining the correct value from $\boldsymbol{\sigma}_{\text{Diff}}(\lambda_0) = 0$. In this case, the correct value is $\lambda_0 = 0.795$, which means that the deformation gradient tensor compatible with the deformation after removal of the electric field is

$$\mathbf{F}^0_{E=150 \frac{\text{MV}}{\text{m}}} = \begin{pmatrix} 0.795 & 0 & 0 \\ 0 & 1.121 & 0 \\ 0 & 0 & 1.121 \end{pmatrix}. \quad (132)$$

This result is counterintuitive when considering that, in this case, chains at greater inclinations become longer. However, when considering the monomer orientation, it is reasonable to assume that some will become more inclined with respect to the electric field as it is

pics for experimental work 16.1.2020/lambda 0 deformation

Figure 14: $\sigma_{\text{Diff}} = \sigma_{\text{EE}} - \sigma_{\text{YY}}$ as a function of λ_0 after the removal of the electric field with the magnitude of $E = 150 \frac{\text{MV}}{\text{m}}$.

pics for experimental work 16.1.2020/mechanical stress

Figure 15: The deviatoric mechanical stress as a function of the deformation ratio, λ . Dashed curves corresponds to the isotropic polymer, continuous curves to the biased polymer and the dot-dashed curves to a polymer described by the IED model. The blue curves corresponds to the normal stress in the direction of the electric field, $\sigma_{\text{EE}}^{\text{m}}$, and the red curves to the transverse stress, $\sigma_{\text{YY}}^{\text{m}} = \sigma_{\text{ZZ}}^{\text{m}}$.

removed. Thus, the polymer will undergo a planar expansion. The end-to-end length and inclination of the chains in the relaxed state, which from now on will be the starting point for each chain examined in a biased polymer, can be deduced from $\mathbf{r}_j = \mathbf{F}^0 \mathbf{r}_j^0$. Note also that the same calculations for the isotropic case yield $\lambda_0^{\text{Iso}} = 1$, as expected.

4.4 Material properties

(Note: mechanical and electrostatic properties - new polymer + comparison)

Given the chain orientations for the example mentioned, the properties of the biased polymer can be examined and compared with the case of an isotropic polymer, which is detailed in Sec. 3.4.1. The polymer's mechanical properties can be assessed by evaluating the mechanical stresses as a function of deformation ratio λ , according to Eq. (124). The calculation of the mechanical stress was done by taking into account and averaging the stresses at $0 \leq \Phi < 2\pi$ with a discretization of $\Delta\Phi = \frac{\pi}{16}$ for each inclination Θ with respect to the electric field and evaluating the stresses for each deformation ratio while taking into account the fraction of each inclination [Eq. (116)] for each case of deformation. Figure 15 presents the mechanical stresses in the direction of the electric field and in the transverse plane as a function of deformation ratio for the isotropic polymer, the biased polymer, and the IED model.

The electrostatic properties can be assessed by first evaluating the polarization of the polymer as a function of the magnitude of the electric field. These calculations are performed following the same steps as for the stress calculations. Figure 16 shows the susceptibilities of the biased polymer, isotropic polymer, and the IED model as a function of electric field, as calculated by using Eq. (129).

Figure 15 shows that applying an electric field during polymerization changes the stress. More precisely, the stress of the biased polymer increases relative to that of the

Figure 16: The susceptibilities of the polymers as a function of the electric field. The black dashed curve corresponds to the isotropic polymer, the black continuous curve to the biased polymer and the black dot-dashed line to a polymer described by the IED model. (the dashed and the continuous curves overlap).

Figure 17: The deformation in the direction of the electric field, λ , as a function of the magnitude of the electric field. The black dashed curve corresponds to the isotropic polymer, the black continuous curve to the biased polymer and the black dot-dashed curves to a polymer described by the IED model.

isotropic polymer, both in the direction of the electric field and perpendicular to it. The stress in the IED model exceeds that in both of the other polymers examined.

Figure 16 shows that the biased polymer and the isotropic polymer have similar susceptibilities. The susceptibilities of both the polymers are initially similar under the excitation a weak electric field (less than $E \cong 5 \frac{\text{MV}}{\text{m}}$) and increase at almost identical rates as the electric field increases. We suspect that the similarity between the susceptibilities of the biased and isotropic polymers stems from the fact that, as the electric field is removed at the end of polymerization, the monomers tend to rearrange in the isotropic polymer whereas the biased polymer deforms. Note that the numerically determined susceptibility of the biased polymer slightly increases relatively to the isotropic polymer, although not enough to visibly separate the curves. The susceptibility of the IED model is independent of the magnitude of the electric field. These results indicate that applying an electric field during polymerization changes the mechanical properties of the polymer more than the electrostatic properties.

4.5 The coupled response

(Note: coupled properties - new polymer + comparison)

After examining and comparing the mechanical and electrostatic properties, we also examine the coupled properties of the biased and isotropic polymers. For this purpose, the main criterion to examine is the deformation λ as a function of the magnitude of the applied electric field (see Fig. 17). As shown in Fig. 17, the deformations in the biased polymer are smaller than those in the isotropic polymer. These results are consistent with the previous results. Figure 16 establishes that the electrostatic response of the biased

polymer does not differ significantly from that of the isotropic polymer, and Fig. 15 shows that the biased polymer is stiffer than the isotropic polymer. Furthermore, the susceptibility of the IED model is constant and generally smaller than for both other polymers within the range of electric fields examined, so the stress in the IED model exceeds that in both other polymers. Thus, it is logical that the deformations in the IED model are smaller than those in the biased and isotropic polymers.

5 Experimental work

A deeper understanding of the electromechanical properties of polymers is required beyond what is provided by our analytical and numerical work.. Therefore, we now present experiments that examine the coupled response of various DEs such as VHB and PDMS and compare their results to analytical calculations. The dielectric constant of the DEs is first determined by calculating the relative permittivity from the capacitance of capacitors containing these DEs as their medium. A common method used to make such measurements is based on the analysis of the capacitance component in an LCR circuit by means of an LCR meter or a capacitance meter.

The experimental work presented below is divided to two main parts: The first part includes an extension of the work presented in ? and examines how the uniaxial and biaxial stretching affects the dielectric constant. The second part presents a new experimental system for measuring the dielectric constant of polymers under an electric field are reports the results for two polymers: VHB 4910 (a commercially available acrylic elastomer from 3M) and polydimethylsiloxane (PDMS, that made in our lab by using the Dow Corning Sylgard 182 Silicone Elastomer Encapsulation Kit). These materials are of interest for their flexibility and accessibility.

5.1 Influence of uniaxial and biaxial stretching

The first experimental system we present allows us to evaluate how uniaxial and biaxial stretching of DEs affects their dielectric constant and to deepen the examination of the dependence of the dielectric constant on deformation. The experimental system was built from a self-constructed stretching device with four movable grippers, shown in Fig. 18a. To measure the relative permittivity of the deformed samples, a C-shaped clamp serving as a plate capacitor (Fig. 18b) was connected to an Agilent U1701A capacitance meter. The

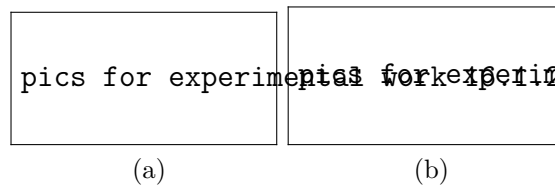


Figure 18: (a) The self constructed stretching device. (b) The C-clamp used as a parallel plate capacitor.

experimental relative permittivity of each sample is calculated by using

$$\epsilon_{r_{Exp}} = \frac{C_s d}{A \epsilon_0}, \quad (133)$$

pics for experimental work 16.1.2020/pdms uniaxial1.2.20

(a)

pics for experimental work 16.1.2020/vhb uniaxial1.2.20

(b)

pics for experimental work 16.1.2020/vhb biaxial1.2.20

(c)

Figure 19: The relative permittivity measurements as functions of the percentage of surface area expansion. The dashed and dotted curves correspond to the analytical results [?], as n are estimated from the stretch at failure (n_f) and from fitting the analytical equations to the experimental results (n_e), respectively. (a) PDMS under uniaxial stretch. (b) VHB under uniaxial stretch. (c) VHB under biaxial stretch.

where C_s is the measured capacitance, d and A are the thickness and surface area of the capacitor, respectively, and ϵ_0 is the vacuum permittivity. The analytical relative permittivity for uniaxial stretching of the dielectric elastomers is calculated by using ?

$$\epsilon_{r_U} = 1 + \chi_0 \left[1 - \frac{1}{5n} \left(\lambda^2 - \frac{1}{\lambda} \right) \right]. \quad (134)$$

The analytical relative permittivity is calculated herein based on the results of ? for the case of biaxial stretching. The final expression is

$$\epsilon_{r_B} = 1 + \chi_0 \left[1 - \frac{2}{5n} \left(\lambda^2 - \frac{1}{\lambda^4} \right) \right], \quad (135)$$

where n is the number of monomers in a single chain, χ_0 is the initial susceptibility, and λ is the magnitude of the uniaxial or biaxial stretching.

Figure 19 presents the results of the experiments and the analytical calculations of the relative permittivity as a function of the percentage of surface area expansion for uniaxial stretching of PDMS (Fig. 19a), uniaxial stretching of VHB 4910 (Fig. 19b), and biaxial stretching of VHB 4910 (Fig. 19c). The analytical results for uniaxial and biaxial stretching are also presented for the different cases examined. The number of monomers in a single chain is estimated from the stretch at failure, which is presumed to be the lock-up stretch and is labeled n_f , and by fitting the analytical equations to the experimental results n_e , as shown in Table 1.

The results show that stretching the samples decreases their thickness decreases relative permittivity. The incompressibility assumption was also examined and, for PDMS,

Table 1: The number of monomers in a single chain for the case presented in Fig. 19.

	PDMS - Uniaxial	VHB - Uniaxial	VHB - Biaxial
n_f	4.35	80	80
n_e	5.844	21.807	5.156

pics for experimental work 16.1.2020/drawing of the s

Figure 20: A schematic description of the experimental system.

the results of both the measured and the calculated thickness are shown. The incompatibility of the curves based on the number of monomers in a polymer chain from the stretch at failure may stem from the fact that the stretch at failure is not necessarily the lock-up stretch of the chain.

5.2 Influence of electric field

The goal of this experimental work was to examine how electric fields of varying magnitude affect the dielectric properties of various polymers. Toward that end, we present a new experimental system that allows us to evaluate variations in dielectric constant as a function of applied electric field. Furthermore, we continue the work of ? and deepen the examination of how the dielectric constant depends on the deformation by examining pre-stretched samples.

5.2.1 Experimental setup

(Note: Samples description)

(Note: Presenting the experimental system)

Ten rectangular samples of each of the two chosen polymers were cut for each examination. For pre-stretched VHB, the samples were then stretched by using a self-constructed stretching apparatus consisting of two movable grippers, as shown in Fig. 18a.

This experimental system was built from nonconductive materials except for the two 30-mm-diameter electrodes that were made of copper and acted as one of two capacitors connected in series, as shown in Fig. 20. The two electrodes were each held in a 60-mm-diameter Teflon housing, as shown in Fig 21. The plate capacitor contained the elastomer sample under examination, and the second capacitor consisted of a fixed TDK UHV-241A capacitor suitable for high voltage.

Figure 21: The parts of the plate capacitore.

To examine pre-stretched samples, we first used a bidirectional stretching apparatus to generate the required tension. After stretching, the sample was held in the stretched state by using a two-part self-constructed Perspex gripper with a 60-mm-diameter opening in the middle and an O-ring notch to maintain the tension in the sample, as shown in Fig. 21.

To measure the referential permittivity of the different samples, we used the plate capacitor from the experimental system. This measurement was made by connecting the plate capacitor to a capacitance meter before connecting the experimental system to the power source. Furthermore, the distance between the electrodes was measured in each experiment. After obtaining the referential values, the power source was connected to the experimental system. As the supplied potential difference is changed in the power source. The potential difference across the plate capacitor was measured as a function of the potential difference applied by the power source by using a noncontact USSVM2 voltmeter from AlphaLab.

(Note: Presenting the work method or protocol)

To evaluate the relative permittivity of the polymer under electrostatic excitation, conservation of charge is taken into account as follows:

$$Q = C_s V_s = C_0 V_0, \quad (136)$$

where Q is the charge on each capacitor, V_s and C_s are the potential difference across and the capacitance of the examined polymer, and V_0 and C_0 are the potential difference across and the capacitance of the fixed capacitor. Thus,

$$V_t = V_s + V_0 = Q \left(\frac{1}{C_s} + \frac{1}{C_0} \right), \quad (137)$$

where V_t is the total potential difference supplied by the power source. Equation (137) gives

$$C_s = \left(\frac{V_t}{V_s} - 1 \right) C_0, \quad (138)$$

from which the current capacitance of the polymer can be calculated, while the constant C_0 is determined by the data shift and confirmed at the beginning of each experiment by measurements made with the capacitance meter.

The relative permittivity, which is the electrostatic property under investigation, is calculated from the results of the calculated capacitance by using Eq. (133).

pics for experimental work 16.1.2020/PDMS RESULTS 24.

(a)

pics for experimental work 16.1.2020/VHB un and pre s

(b)

Figure 22: The permittivity measurements as functions of the electric field on the sample. The Blue dots corresponds to a relaxed sample and the red circles corresponds to the area pre-stretch of $A = 225\%$. (a) PDMS, (b) VHB.

5.2.2 Results and discussion

In all tests, the sample thickness was measured in order to calculate the relative permittivity by using Eq. (133) and thereby correctly determine the electric field induced in the sample, which is calculated as $E_s = \frac{V_s}{d}$. Measurements of the pre-stretched VHB 4910 confirmed the incompressibility assumption in this case.

The solid blue dots (red open circles) in the two plots of Fig. 22 show the measured relative permittivity as a function of the electric field in the un-stretched samples (2.25 area pre-stretched samples). The error bars show the standard deviation. The results shown in Sec. 5.1 are consistent with the current results as $E_s \rightarrow 0$. For the VHB 4910 samples (Fig. 22b), the relatively small standard deviation of the different measurements provides confidence in the accuracy of the measurements for this material. The relatively large standard deviation of the PDMS samples may be attributed to the fact that the samples were made manually in our lab, although a clear trend appears in the results. The relative permittivity of the two polymers examined increases with the magnitude of the electric field.

The variations in the responses of the two polymers examined hints that they are governed by the polymer microstructure. Furthermore, the results of the pre-stretched VHB 4910 provides more evidence of the role of the microstructure. Given that the initial value of the relative permittivity corresponds to the results shown in Fig. 19, the maximum relative permittivity measured in the pre-stretched case is much less than that measured in the relaxed case, despite the fact that a stronger electric field was achieved in the thinner samples. The results for both polymers (Fig. 22) show that the rate of change in relative permittivity is much greater at relatively low electric fields ($< 1 \frac{\text{MV}}{\text{m}}$). Thus, additional experimental analyses of the relationship between the microscopic structure and the macroscopic response are needed to understand the coupled electromechanical behavior of different polymers.

6 Conclusions

(Note: Opening - Motivation)

This thesis presents another step toward the use of DEs in a wide range of applications and comes at a time when we are seemingly ready for such advances in different fields, such as clean energy, medicine, and robotics. Thus, given that a substantial improvement in the electromechanical response of DEs is required, we present a possible method for influencing and analyzing the response of these materials and their structure and properties, all without adding any foreign material.

(Note: 3. Electroelasticity of solutions and anisotropic networks of polymer molecules)

(Note: 3.1 general - multiscale analysis)

To begin, we carried out a multiscale analysis of the electromechanical coupling in DEs for several hierarchical cases, from a single electric charge to a network. The analysis applies the conservation of energy through the first law of thermodynamics in terms of the electric enthalpy and the entropy of a system subjected to an electric field. The analysis of the polymer microstructure is based on statistical mechanics, and we assume that each chain is in the most probable configuration.

(Note: 3.2 an analysis of the isotropic chain end-to-end length, tau and force)

We then analyze the polymer chain in the case of no electric field. This analysis yields the relationship between the Lagrange multiplier τ , which can be understood as the chain's mechanical constraint, and the normalized end-to-end length of the chain through the Langevin function. The calculations also determine the end-to-end length of a chain in such a case, which is similar to that obtained by ?? and ? but differs from the commonly used result based on random walk statistics [???]. In addition, we deduce a relation between the end-to-end length of a chain and the external force exerted on the chain.

(Note: 3.3 polymer chains in an electric field and monomers distribution)

To examine the proposed method for controlling the electro-elastic modulus of a polymer network by polymerizing under an electric field, we develop an approach to determine the most probable configuration for each group of polymer chains and for the orientational distribution of the monomers in such a case.

(Note: 3.4 an anisotropic network analysis - general analysis with a reference for polymerization under an electric field + material properties)

Next, we derive an expression for the total entropy of the polymer that allows us to evaluate the distribution and the fraction of the chains in the different chain groups. Given these fractions, expressions for the mechanical stress and the polarization are derived in order to determine the polymer response.

(Note: 4. Application to electrostatically biased network - reminded our main idea for the

polymerization)

To examine the outcome of our proposed polymerization under an electric field, which leads to a “biased” polymer, we applied a numerical analysis based on our analytical work, and the predictions of this analysis are compared with the experimental results for an isotropic polymer and for the IED model.

(**Note:** 4.1 chain end-to-end length - isotropic case (our analysis is more accurate) and anisotropic (mention the examined parameters))

The initial step of the numerical analysis involves examining the results for the end-to-end length of a chain in an isotropic polymer. For the biased polymer, the chain configuration is compared for three parameters: the maximum number of chain configurations, the most probable end-to-end length, and the Lagrange multiplier τ that relates to the end-to-end length to the maximum number of configurations. The results indicate that the electric fields less than $50 \frac{\text{MV}}{\text{m}}$ produce negligible differences with respect to the isotropic case. However, upon increasing the electric field, the end-to-end length of chains increases for all inclinations, which is counterintuitive because uniaxial dipolar monomers tend to rotate in the direction of the electric field.

(**Note:** 4.2 monomer orientation - aspire to be as in the amorphous case)

The results of the investigation of the monomer orientation for chains at various inclinations with respect to the electric field and the comparison with the monomer distribution in the amorphous case shows that, despite their constraints, monomers in chains tend to orient as though they were unattached.

(**Note:** 4.3 assessing the free state and discussing the chains distribution/weights)

Next, the free state of the biased polymer was assessed. This state occurs when the deviatoric stress vanishes and the body is in a stress-free configuration. The results show that the biased polymer contracts in the direction of the applied electric field, which improves our understanding of the importance to polymer properties of the microscopic structure because, when the electric field is turned off, the monomers rotate away from its direction, which leads to contraction in the given direction. The spatial expansion in the transverse direction is due to incompressibility.

(**Note:** 4.4 the material properties and coupled response)

The resulting material properties differ from the mechanical properties, as manifested by the biased polymer being stiffer than the isotropic polymer. No significant difference in the electrostatic properties are found between the two polymers. However, in both cases the susceptibility appears to vary as a function of electric-field magnitude. The analysis of the coupled response establishes that the electromechanical response of the biased polymer is less than that of the isotropic polymer, which is consistent with the mechanical and electrostatic properties of both polymers.

(**Note:** 5. Experimental work)

The results of the present experimental work imply that the dependence of the dielectric properties of the polymers on the deformation and the electric-field magnitude cannot be neglected. Moreover, they suggest that common models that assume constant relative permittivity, such as the models of ? and ?, are not applicable if the polymer is subjected to different mechanical loads or exposed to an electric field at different magnitudes. Additionally, our extension to the model of ? for the case of biaxial stretching predicts the relationship between relative permittivity, which reflects the dielectric behavior, and polymer deformation. However, the assessment of the number of monomers in a single chain from the stretch at failure is insufficient to predict these relationships, which may stem from the fact that the stretch at failure is not necessarily the lock-up stretch of the chain. Furthermore, our examination of how electric fields of varying magnitude affect the dielectric properties reveals the differences in the responses of the relaxed and pre-stretched VHB 4910, thereby demonstrating the prominent influence of the microscopic structure on the macroscopic electromechanical behavior. Accordingly, pre-stretching the sample is found to hinder the evolution of the relative permittivity as the magnitude of the electric field increases.

(Note: ** Future work)

We have spent considerable time pondering the future directions of this research. Although this thesis presents a method of tuning polymer properties, it has so far been applied only to the case of uniaxial dipoles. Thus, spontaneous and transversely isotropic dipoles should also be analyzed. In addition, the creation of a biased polymer should be examined from different directions and with electric fields of greater magnitude to determine the threshold field above which significant differences appear in the electrostatic properties vis à vis the isotropic polymer. Moreover, how an electric field affects the dielectric properties should be experimentally examined for additional materials, with more pre-stretching conditions and under higher-magnitude electric fields.

References

Appendix

A The first law of thermodynamics in terms of electric enthalpy

The first law of thermodynamics is $\dot{U} = \dot{W}_0 + \dot{Q}$ [Eq. (7)] [??], where

$$\dot{U} = \frac{d}{dt} \int_{V_0} u(\mathbf{F}, \mathbf{P}) dV_0 + \frac{d}{dt} \int_{\mathbb{R}^3} \frac{\epsilon_0}{2} \mathbf{E} \cdot \mathbf{E} dV, \quad (139)$$

and the system is assumed to not to interact with other bodies and the electric fields is assumed to vanish far from the system. The rate of work done by mechanical loads through deformation and by the electric field through variations in charge is [??]

$$\frac{dW_0}{dt} = \int_V b_i v_i dV + \int_{\partial V} t_i v_i dA + \int_V \phi \frac{d}{dt} (q dV) + \int_{\partial V} \phi \frac{d}{dt} (\rho_a dA). \quad (140)$$

Using the definition of the electric enthalpy density [?],

$$h(\mathbf{F}, \mathbf{E}) = u(\mathbf{F}, \mathbf{P}) - J\mathbf{P} \cdot \mathbf{E}, \quad (141)$$

gives

$$\begin{aligned} \dot{U} &= \frac{d}{dt} \int_{V_0} h(\mathbf{F}, \mathbf{E}) dV_0 + \frac{d}{dt} \int_{V_0} \mathbf{P} \cdot \mathbf{E} J dV_0 + \frac{d}{dt} \int_{\mathbb{R}^3} \frac{\epsilon_0}{2} \mathbf{E} \cdot \mathbf{E} dV \\ &= \frac{d}{dt} \int_{V_0} h(\mathbf{F}, \mathbf{E}) dV_0 + \frac{d}{dt} \int_V \mathbf{P} \cdot \mathbf{E} dV + \frac{d}{dt} \int_{\mathbb{R}^3} \frac{\epsilon_0}{2} \mathbf{E} \cdot \mathbf{E} dV. \end{aligned} \quad (142)$$

In the body $\mathbf{D} = \mathbf{P} + \epsilon_0 \mathbf{E}$ and outside the body $\mathbf{D} = \epsilon_0 \mathbf{E}$, so

$$\dot{U} = \frac{d}{dt} \int_{V_0} h(\mathbf{F}, \mathbf{E}) dV_0 + \frac{d}{dt} \int_{\mathbb{R}^3} (\mathbf{D} - \epsilon_0 \mathbf{E}) \cdot \mathbf{E} dV + \frac{d}{dt} \int_{\mathbb{R}^3} \frac{\epsilon_0}{2} \mathbf{E} \cdot \mathbf{E} dV. \quad (143)$$

Thus, we have

$$\dot{U} = \frac{d}{dt} \int_{V_0} h(\mathbf{F}, \mathbf{E}) dV_0 - \frac{d}{dt} \int_{\mathbb{R}^3} \frac{\epsilon_0}{2} \mathbf{E} \cdot \mathbf{E} dV + \frac{d}{dt} \int_{\mathbb{R}^3} \mathbf{D} \cdot \mathbf{E} dV. \quad (144)$$

Define $\dot{H} = \frac{d}{dt} \int_{\Omega_0} h(\mathbf{F}, \mathbf{E}) dV_0$ as the stored electric enthalpy in the body. The first law of thermodynamics then gives

$$\dot{H} - \frac{d}{dt} \int_{\mathbb{R}^3} \frac{\epsilon_0}{2} \mathbf{E} \cdot \mathbf{E} dV = \dot{W}_0 + \dot{Q} - \frac{d}{dt} \int_{\mathbb{R}^3} \mathbf{D} \cdot \mathbf{E} dV. \quad (145)$$

Consider the last term

$$-\frac{d}{dt} \int_{\mathbb{R}^3} \mathbf{D} \cdot \mathbf{E} dV = \frac{d}{dt} \int_{\mathbb{R}^3} \mathbf{D} \cdot \nabla \phi dV = \frac{d}{dt} \int_{\mathbb{R}^3} \nabla \cdot (\mathbf{D} \phi) dV - \frac{d}{dt} \int_{\mathbb{R}^3} \nabla \cdot \mathbf{D} \phi dV. \quad (146)$$

Assuming no free charges outside the body, then $\nabla \cdot \mathbf{D} = q$ in the body and zero outside, so

$$-\frac{d}{dt} \int_{\mathbb{R}^3} \mathbf{D} \cdot \mathbf{E} dV = \frac{d}{dt} \int_{\partial V} \phi \mathbf{D} \cdot \hat{\mathbf{n}} dA - \frac{d}{dt} \int_V \phi q dV, \quad (147)$$

where we make use of the divergence theorem and exploit the assumption that the electric field vanishes at distance. Thus,

$$-\frac{d}{dt} \int_{\mathbb{R}^3} \mathbf{D} \cdot \mathbf{E} dV = -\frac{d}{dt} \int_{\partial V} \phi \rho_a dA - \frac{d}{dt} \int_V \phi q dV. \quad (148)$$

The last term can be simplified to

$$\begin{aligned} -\frac{d}{dt} \int_V \phi q dV &= -\frac{d}{dt} \int_{V_0} \phi q J dV_0 = -\int_{V_0} \dot{\phi} q J dV_0 - \int_{V_0} \phi \frac{d}{dt} (q J dV_0) \\ &= -\int_V \dot{\phi} q dV - \int_V \phi \frac{d}{dt} (q dV). \end{aligned} \quad (149)$$

The first term of Eq. (148) is

$$-\frac{d}{dt} \int_{\partial V} \phi \rho_a dA = -\frac{d}{dt} \int_{\partial V_0} \phi \rho_a^0 dA_0, \quad (150)$$

where ρ_a^0 is the referential surface charge such that $\rho_a^0 dA_0 = \rho_a dA$. Thus,

$$-\frac{d}{dt} \int_V \phi q dV = -\int_{\partial V_0} \dot{\phi} \rho_a^0 dA_0 - \int_{\partial V_0} \phi \frac{d}{dt} (\rho_a^0 dA_0) = -\int_{\partial V} \dot{\phi} \rho_a dA - \int_{\partial V} \phi \frac{d}{dt} (\rho_a dA). \quad (151)$$

Substituting this relation into Eq. (148) gives

$$-\frac{d}{dt} \int_{\mathbb{R}^3} \mathbf{D} \cdot \mathbf{E} dV = -\int_{\partial V} \dot{\phi} \rho_a dA - \int_{\partial V} \phi \frac{d}{dt} (\rho_a dA) - \int_V \dot{\phi} q dV - \int_V \phi \frac{d}{dt} (q dV), \quad (152)$$

and using this relation in the first law of thermodynamics [Eq. (145)] and the expression for the external work W_0 [Eq. (140)] gives

$$\begin{aligned} \dot{H} - \frac{d}{dt} \int_{\mathbb{R}^3} \frac{\epsilon_0}{2} \mathbf{E} \cdot \mathbf{E} dV &= \int_V \phi \frac{d}{dt} (q dV) + \int_{\partial V} \phi \frac{d}{dt} (\rho_a dA) + \dot{Q} + \int_V b_i v_i dV + \int_{\partial V} t_i v_i dA \\ &\quad - \int_{\partial V} \dot{\phi} \rho_a dA - \int_{\partial V} \phi \frac{d}{dt} (\rho_a dA) - \int_V \dot{\phi} q dV - \int_V \phi \frac{d}{dt} (q dV) \\ &= \dot{Q} - \int_{\partial V} \dot{\phi} \rho_a dA - \int_V \dot{\phi} q dV + \int_V b_i v_i dV + \int_{\partial V} t_i v_i dA. \end{aligned} \quad (153)$$

In terms of the external work due to the variations in the electric potential [??],

$$\frac{dW}{dt} = \int_V b_i v_i dV + \int_{\partial V} t_i v_i dA - \int_{\partial V} \dot{\phi} \rho_a dA - \int_V \dot{\phi} q dV, \quad (154)$$

we finally obtain the expression for the first law of thermodynamics in terms of the electric enthalpy:

$$\dot{H} - \frac{d}{dt} \int_{\mathbb{R}^3} \frac{\epsilon_0}{2} \mathbf{E} \cdot \mathbf{E} dV = \dot{W} + \dot{Q}. \quad (155)$$

B Chain stress and deriving the chain end-to-end vector from the deformation gradient

To evaluate the stress(see discussion in Sec. 3.4.1), we first derive the term $\frac{\partial \mathbf{r}}{\partial \mathbf{F}}$. This is done using index notation.

The end-to-end vector of the chain in the current configuration is

$$r_i = F_{ip} r_p, \quad (156)$$

where r_i^0 is the end-to-end vector of the chain in the reference configuration and F_{ij} is the deformation gradient. Accordingly,

$$\frac{\partial r_i}{\partial F_{kl}} = \frac{\partial}{\partial F_{kl}} (F_{ip}) r_p^0 = \delta_{ik} \delta_{lp} r_p^0 = \delta_{ik} r_l^0. \quad (157)$$

From Eq. (124), the mechanical stress in chain j is

$$\sigma_{ks}^{m(j)} = \frac{kT}{l} \left(\tau_i^{(j)} \frac{\partial r_i^{(j)}}{\partial F_{kl}} \right) F_{sl} = \frac{kT}{l} \tau_i^{(j)} \delta_{ik} \delta_{lp} r_p^{0(j)} F_{sl} = \frac{kT}{l} \tau_k^{(j)} F_{sp} r_p^{0(j)} = \frac{kT}{l} \tau_k^{(j)} r_s^{(j)}. \quad (158)$$

Since $\tau_k^{(j)} \parallel r_s^{(j)}$ (established in Sec. 3.2.3), it follows that

$$\sigma_{ks}^{m(j)} = \frac{kT}{l} \tau^{(j)} r^{0(j)} \hat{r}_k^{(j)} \hat{r}_s^{(j)}. \quad (159)$$

C The initial guess for $\boldsymbol{\tau}$

The Lagrange multiplier $\boldsymbol{\tau}$ is extracted from the implicit equation that follows from the constraint given by Eq. (98),

$$\int \hat{\boldsymbol{\xi}} p d\Gamma = \frac{\mathbf{r}}{nl}, \quad (160)$$

where

$$p(\hat{\boldsymbol{\xi}}, h) = \frac{1}{Z} \exp\left(\boldsymbol{\tau} \cdot \hat{\boldsymbol{\xi}} - \frac{h}{kT}\right). \quad (161)$$

Taking the first two terms of the Taylor-series expansion for $\boldsymbol{\tau}$ gives

$$\boldsymbol{\tau} = \boldsymbol{\tau}_0 + \mathbf{A}\mathbf{r} + o(r^2) \cong \mathbf{A}\mathbf{r}, \quad (162)$$

where according to Eq. (75) $\boldsymbol{\tau}_0 = \boldsymbol{\tau}(r=0) = 0$.

Thus,

$$\exp\left[\boldsymbol{\tau}(\mathbf{r}) \cdot \hat{\boldsymbol{\xi}} - \frac{h}{kT}\right] \xrightarrow{\mathbf{E} \rightarrow 0} \exp(\hat{\boldsymbol{\xi}} \cdot \mathbf{A}\mathbf{r}) \cong 1 + A_{ik}\hat{\xi}_i r_k, \quad (163)$$

and

$$Z = \int_{\theta, \phi} (1 + A_{ik}\hat{\xi}_i r_k) \sin(\theta) d\theta d\phi = 4\pi + A_{ik} \int \hat{\xi}_i d\Gamma r_k = 4\pi. \quad (164)$$

Thus,

$$p(\hat{\boldsymbol{\xi}}, h) = \frac{1}{Z} \exp\left(\boldsymbol{\tau} \cdot \hat{\boldsymbol{\xi}} - \frac{h}{kT}\right) = \frac{1}{4\pi} (1 + (\mathbf{A}\mathbf{r}) \cdot \hat{\boldsymbol{\xi}}), \quad (165)$$

and by taking using Eq. (165) in Eq. (160) we obtain

$$\begin{aligned} \frac{1}{4\pi} \int \hat{\boldsymbol{\xi}} (1 + (\mathbf{A}\mathbf{r}) \cdot \hat{\boldsymbol{\xi}}) d\Gamma &= \frac{1}{4\pi} \int (\mathbf{A}\mathbf{r}) \cdot \hat{\boldsymbol{\xi}} \otimes \hat{\boldsymbol{\xi}} d\Gamma = \frac{1}{4\pi} \left(\frac{4\pi}{3} \mathbf{I}\right) \cdot (\mathbf{A}\mathbf{r}) \\ &= \frac{1}{3} (\mathbf{A}\mathbf{r}) \cdot \mathbf{I} = \frac{\mathbf{r}}{nl} \implies \mathbf{A} = \frac{3}{nl} \mathbf{I}. \end{aligned} \quad (166)$$

Finally, using $\boldsymbol{\tau}(\mathbf{E} \rightarrow \mathbf{0})$ gives

$$\boldsymbol{\tau} = \mathbf{A}\mathbf{r} = \frac{3\mathbf{r}}{nl}. \quad (167)$$